

AD-A284 387



(1)

ARMY RESEARCH LABORATORY

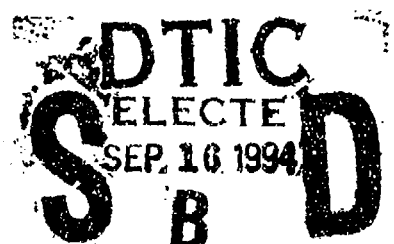


# **Effect of Heat Treatment on the Microstructure and Properties of AerMet® 100 Steel**

John H. Graves

ARL-TR-507

August 1994



94-29973



DTIC QUALITY INSPECTED 3

Approved for public release; distribution unlimited.

94 9 15 029

The findings in this report are not to be construed as an official Department of the Army position unless so designated by other authorized documents.

Citation of manufacturer's or trade names does not constitute an official endorsement or approval of the use thereof.

Destroy this report when it is no longer needed. Do not return it to the originator.

# **Effect of Heat Treatment on the Microstructure and Properties of AerMet® 100 Steel**

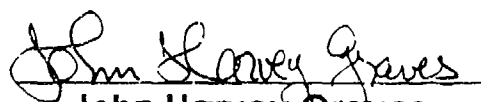
A Thesis Submitted to the Faculty of the

**Worcester Polytechnic Institute**

in Partial Fulfillment of the  
Requirements for the Degree

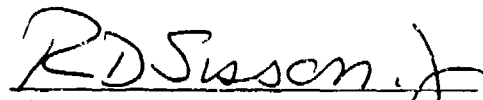
**Master of Science in Materials Engineering**

by

  
**John Harvey Graves**

May 1994

Approved by:

  
**Richard D. Sisson Jr., Advisor and  
Materials Science and Engineering Program Head**

  
**M.N. Noori, Mechanical Engineering Department Head**

REPORT DOCUMENTATION PAGE			Form Approved OMB No. 0704-0188
<p>Public reporting burden for this collection of information is estimated to average 1 hour per response, including the time for reviewing instructions, searching existing data sources, gathering and maintaining the data needed, and completing and reviewing the collection of information. Send comments regarding this burden estimate or any other aspect of this collection of information, including suggestions for reducing this burden, to Washington Headquarters Services, Directorate for Information Operations and Reports, 1215 Jefferson Davis Highway, Suite 1204, Arlington, VA 22202-4302, and to the Office of Management and Budget, Paperwork Reduction Project (0704-0188), Washington, DC 20503.</p>			
1. AGENCY USE ONLY (Leave blank)	2. REPORT DATE	3. REPORT TYPE AND DATA'S COVERED	
	August 1994	Final Report	
4. TITLE AND SUBTITLE  Effect of Heat Treatment on the Microstructure and Properties of AerMet® 100 Steel		6. FUNDING NUMBERS	
6. AUTHOR(S)  John H. Graves			
7. PERFORMING ORGANIZATION NAME(S) AND ADDRESS(ES)  U.S. Army Research Laboratory Watertown, MA 02172-0001 ATTN: AMSRL-MA-CC		8. PERFORMING ORGANIZATION REPORT NUMBER	
9. SPONSORING/MONITORING AGENCY NAME(S) AND ADDRESS(ES)  U.S. Army Research Laboratory 2800 Powder Mill Road Adelphi, MD 20783-1197		10. SPONSORING/MONITORING AGENCY REPORT NUMBER  ARL-TR-507	
11. SUPPLEMENTARY NOTES  Thesis submitted to Worcester Polytechnic Institute in partial fulfillment of the requirements for the Degree - Master of Science in Materials Engineering, May 1994.			
12a. DISTRIBUTION/AVAILABILITY STATEMENT  Approved for public release; distribution unlimited.		12b. DISTRIBUTION CODE	
13. ABSTRACT (Maximum 200 words)  (See reverse, page ii.)			
DOD QUALITY INSPECTED 3			
14. SUBJECT TERMS  Armor, Adiabatic shear, Secondary hardening, Steel		15. NUMBER OF PAGES 74	
		16. PRICE CODE	
17. SEC. / CLASSIFICATION OF REPORT  Unclassified	18. SECURITY CLASSIFICATION OF THIS PAGE  Unclassified	19. SECURITY CLASSIFICATION OF ABSTRACT  Unclassified	20. LIMITATION OF ABSTRACT  UL

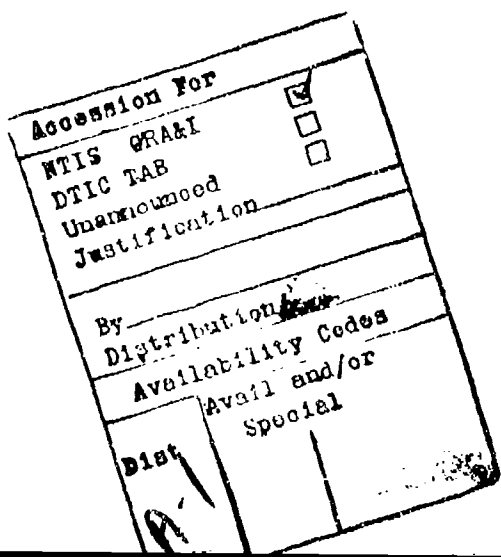
# **Effect of Heat Treatment on the Microstructure and Properties of AerMet® 100 Steel**

**by John Harvey Graves**

## **Abstract**

Results from mechanical, ballistic, and stress corrosion cracking experiments indicate that AerMet® 100 Steel is well suited for applications that require both load-bearing capability, ballistic tolerance, and resistance to stress corrosion cracking. For applications where ballistic tolerance is the primary design criterion, an alternate heat treatment of AerMet® 100 produces markedly improved ballistic performance while retaining adequate toughness for use in less exacting structural applications. The findings of this study also indicate that as hardness is increased, concomitant increases in fracture toughness will be required to advance the performance capabilities of steels used for ballistic applications against small caliber projectiles.

The stress corrosion cracking resistance of standard condition AerMet® 100 as measured using a cantilever bend apparatus is greater than conventional high strength steels by 50% to 100%. However, AerMet® 100 is sensitive to aging temperature, as demonstrated by stress corrosion tests on specimens processed using an alternate heat treatment. The impressive combination of ballistic tolerance and stress corrosion resistance found in AerMet® 100 make it ideally suited for use in demanding structural applications. Moreover, the range of properties that can be achieved using alternate heat treatments provide a degree of flexibility not found in other high strength steels.



## Acknowledgments

I gratefully acknowledge the following people for their respective contributions to this program of research:

Ballistic Testing	James Brown*
Mechanical Testing	Robert Pasternak*
	Karen Harvey*
	John Saccoccio*
	Francis Muncey*
Thermal Treatment	Francis Hanrahan*
Technical Support	John V. Kelley II*
Technical Discussion	Ralph P.I. Adler*
	Eric B. Kula*
	Raymond Hemphill†
	Thomas McAffrey†
	Heather Wickman*
	Charles Hickey*
	Morris Azrin*
	Paul Buckley*
	John Beatty*
	Richard Brown°
Specimen Preparation	Leonard Bucciarelli*
Photographs	Jeffrey Loughlin*

The Materials Directorate of the U.S. Army Research Laboratory provided funding, materials, laboratory space, and equipment without which this program would not have been possible.

To Professor Richard Sisson, my thesis advisor, I extend particular thanks for his thoughtful contributions and the extraordinary degree of freedom he afforded me during the completion of this research program.

My two year old son Matthew deserves special recognition for his unique contribution. Matthew was always eager to 'help' his father type on the computer, correct the manuscript with colorful crayola crayons, and discard any portions of the manuscript that did not meet his exacting standards.

To Suzanne, my wife, I express my thanks for continued support during the completion of the Master's Degree and for occupying our enthusiastic son during the many evenings and weekends required to complete data analysis and prepare the manuscript.

\* U.S. Army Research Laboratory, Watertown, Massachusetts

† Carpenter Technology Corporation, Reading, Pennsylvania

° University of Rhode Island

# Table of Contents

Abstract .....	ii
Acknowledgments .....	iii
List of Tables .....	vi
List of Figures .....	vii
Nomenclature .....	viii
1.0 Introduction .....	1
2.0 Background .....	2
Secondary Hardening Steels .....	2
High Yield 180 .....	4
Air Force 14 Cobalt - 10 Nickel (AF 1410) .....	5
AerMet® 100 .....	5
Alloying Elements .....	5
Carbon .....	6
Nickel .....	6
Cobalt .....	6
Molybdenum .....	6
Chromium .....	7
Rare Earth Additions .....	7
Stress Corrosion Cracking .....	7
3.0 Research Program .....	9
4.0 Experimental Procedures .....	10
Material and Processing .....	10
Development of Ageing Curves .....	10
Short Range Order Experiment .....	12
Mechanical Properties .....	13
Stress Corrosion Cracking Tests .....	13
Processing of Ballistic Plate .....	18
Ballistic Tests .....	18

## Table of Contents

5.0 Experimental Results .....	20
Solution Treatment .....	20
Ageing Study .....	20
Short Range Order Experiment .....	22
Mechanical Properties .....	23
Stress Corrosion Cracking Tests .....	24
Ballistic Tests .....	25
6.0 Discussion .....	27
Processing and Properties .....	27
Ballistic Tests .....	27
Stress Corrosion Cracking Tests .....	30
7.0 Conclusions and Recommendations .....	33
References .....	34
Appendix A .....	A-1
Appendix B .....	B-1

## List of Tables

Table 1	Properties of Three Secondary Hardening Steels .....	3
Table 2a	Composition Ranges of Three Secondary Hardening Steels .....	4
Table 2b	Typical Alloy Chemistry of Three Secondary Hardening Steel.....	4
Table 3	Chemical Analysis of AerMet® 100 Heat 89557 by Weight Percent .....	10
Table 4	AerMet® 100 Chemistry Requirements from AMS Specification 6532 .....	11
Table 5	Manufacturer's Certified Properties for Heat 89557 .....	11
Table 6	Heat Treatments Selected for Ballistic Plates .....	21
Table 7	Measured Mechanical Properties of AerMet® 100 Steel .....	23
Table 8	Comparison of ARL•MD Cantilever Beam and Atrens' Linear Increasing Stress Test Data .....	32

## List of Figures

Figure 1	Cantilever Beam Specimen Used for Stress Corrosion Cracking Tests .....	14
Figure 2	Cantilever Beam Specimen Mounted in Corrosion Cell .....	15
Figure 3	Schematic of Cantilever Beam Apparatus.....	16
Figure 4a	Cantilever Beam Apparatus .....	17
Figure 4b	Specimen Mounted in Cantilever Beam Apparatus .....	17
Figure 5	Definition of Partial and Complete Penetration.....	19
Figure 6	Effect of Solution Treatment Temperature on the As Cooled Hardness of AerMet® 100 .....	20
Figure 7	Results of AerMet® 100 Ageing Study.....	21
Figure 8	Hardness and Strength as a Function of Ageing Time for a Two Step Ageing Treatment.....	22
Figure 9	Results of Cantilever Beam Stress Corrosion Cracking Tests.....	24
Figure 10	Results of 0.30 Caliber AP M2 Ballistic Tests on AerMet® 100 Steel ...	26
Figure 11	Results of 0.50 Caliber AP M2 Ballistic Tests on AerMet® 100 Steel ...	26
Figure 12	Shear Instability Strains for AerMet® 100 Steel for Various Ageing Treatments .....	28
Figure 13	Comparison of Shear Instability Strains for Various High Strength Steels and AerMet® 100.....	29
Figure 14	Atrrens' Crack Velocity Data for AerMet® 100 Steel.....	30

## Nomenclature

A	Matrix-carbide interfacial area
a	Flaw Size
$a_f$	Final Flaw Size (Flaw Size at Failure)
$a_i$	Initial Flaw Size
$\alpha$	Dimensionless parameter for $K_{ISCC}$ specimen
AD	Areal Density
AISI	American Iron and Steel Institute
AMS	Aerospace Material Specification
AP	Armor Piercing (Bullet)
ARL-MD	U.S. Army Research Laboratory Materials Directorate
ASTM	American Society for Testing and Materials
B	$K_{ISCC}$ Specimen Width
CarTec	Carpenter Technology Corporation
CVN	Charpy "V" Notch
DoD	Department of Defense
DPH	Diamond Pyramid Hardness
ESR	Electroslag Remelted
fps	feet per second
$\gamma$	Interfacial energy
$\gamma_i$	Shear Instability Strain
HRC	Rockwell C Hardness
HV	Vickers Hardness
K	Stress Intensity Factor
$K_I$	Mode I Stress Intensity Factor
$K_{IC}$	Critical Mode I Stress Intensity Factor
$K_{ISCC}$	Threshold Mode I Stress Intensity Factor for Stress Corrosion Cracking
LIST	Linear Increasing Stress Test
M	Bending Moment for $K_{ISCC}$ tests
$M_f$	Martensite Finish Temperature
mps	meters per second
$M_s$	Martensite Start Temperature
NAWC	Naval Air Warfare Center
PBL	Protection Ballistic Limit
ppm	Parts per Million

## Nomenclature

Q&T	Quenched and Tempered (Steel)
REM	Rare Earth Modified
SAE	Society of Automotive Engineers
$\sigma_y$	Yield Strength
$t_f$	Time to Failure
V	Volume of a precipitate
$V_{50}$	Velocity associated with a 50% probability of ballistic failure
VAR	Vacuum Arc Remelted
VIM	Vacuum Induction Melted
W	$K_{ISCC}$ Specimen Height
wt%	weight percent
$\Delta G^*$	Activation barrier for heterogeneous nucleation
$\Delta G_d$	Free energy released by the destruction of a defect
$\Delta G_s$	Change in the matrix-carbide misfit strain energy
$\Delta G_v$	Chemical driving force for precipitation
$\Delta H$	Enthalpy of Formation

## 1.0 Introduction

The most desired property for an armor material is high hardness, because hardness is the only measurable mechanical property that consistently correlates well with ballistic performance.<sup>1</sup> Increased hardness levels, however, can result in plate shattering. Thus, for structural components that require ballistic tolerance, the material used must also possess adequate fracture toughness.<sup>2</sup>

For many years, the Army has used low and medium carbon alloy steels for applications on ground vehicles and helicopters that require ballistic tolerance. A component is ballistically tolerant when it can continue to perform its function even after sustaining impacts from kinetic energy penetrators (bullets and fragments). Quenched and tempered (Q&T) grades such as AISI 4340 steel can be heat treated to ultrahigh strength levels while retaining toughness adequate for use in ballistically tolerant components.<sup>3</sup>

Achieving improved ballistic performance requires increasing the hardness of quenched and tempered steels. Since maximum attainable hardness is a function of carbon content, the primary way to increase hardness would be to move to a higher carbon alloy steel. Although increasing carbon content will produce a higher hardness steel, fracture toughness diminishes and ballistic tests reveal a greater propensity towards plate shattering beyond carbon levels of approximately 0.40 to 0.50 weight percent (wt%). It is unlikely, therefore, that we can achieve further significant improvements in the ballistic performance of Q&T steels. Rather, we must turn our attention to other grades of steel.

One possibility that has received only limited attention is the use of secondary hardening steels such as HY 180, AF 1410, and AerMet® 10J. These secondary hardening steels derive their incremental hardness from precipitated carbides in a fine lath martensitic microstructure. The hardness of some precipitation hardening grades is increased further through addition of more nickel and cobalt for solid solution strengthening. Cobalt also provides recovery resistance and raises the Martensite start ( $M_s$ ) temperature of iron based alloys, permitting the addition of more nickel. Nickel lowers the  $M_s$  temperature and improves cleavage resistance, thus enhancing fracture toughness.

## 2.0 Background

### Secondary Hardening Steels

Secondary hardening steels make up a category of quenched and tempered martensitic steels that derive increased hardness from carbide precipitation during stage IV tempering.<sup>4</sup> Stage IV tempering takes place at temperatures ranging from 450°C to 600°C (850°F to 1100°F). Above 450°C (850°F), substitutional diffusion of carbide forming elements such as chromium, vanadium, and molybdenum becomes significant. The mean diffusion distance of carbide forming elements is between 20Å and 50Å, roughly the same size as an alloy carbide nucleus.<sup>5</sup> During stage IV tempering, cementite ( $\text{Fe}_3\text{C}$ ) dissolves, giving way to precipitation and growth of finer alloy carbides.<sup>6</sup>

Transformation of cementite to alloy carbides can take place by in-situ transformation or separately by nucleation and growth.<sup>7</sup> During in-situ transformation, alloy carbides nucleate at ferrite-cementite interfaces and grow until the cementite disappears. Alternatively, alloy carbides can nucleate heterogeneously within the ferrite matrix on dislocations, lath boundaries, and prior austenite grain boundaries. The carbides then grow as the cementite dissolves.

The ability of alloy carbides to increase hardness is related to the volume fraction of carbides and the fineness of the alloy carbide dispersion. The volume fraction of precipitated carbides depends on the solubility of the carbide forming elements in the austenite matrix prior to quenching. The fineness of the carbide dispersion depends on the activation barrier for heterogeneous nucleation,  $\Delta G^*$ :<sup>8</sup>

$$\Delta G^* = -V (\Delta G_V - \Delta G_s) + A\gamma - \Delta G_d \quad (i)$$

where: V is the precipitate volume

$\Delta G_V$  is the chemical driving force for precipitation

$\Delta G_s$  is the change in the matrix-carbide misfit strain energy

A is the matrix-carbide interfacial area

$\gamma$  is the interfacial energy

$\Delta G_d$  is the free energy released by the destruction of a defect

Because the enthalpy of formation<sup>9</sup>,  $\Delta H$ , for alloy carbides is less than that for cementite, there is a thermodynamic driving force that favors replacement of  $M_3C$  carbides with  $M_2C$  carbides, where M stands for an appropriate metallic element. The fact that the  $M_2C$  carbides are an order of magnitude smaller than the  $M_3C$  carbides leads to the most important feature of this class of steels, namely that concomitant increases in fracture toughness and hardness are possible. Although strength and toughness are usually mutually exclusive attributes, the class of secondary hardening steels to which HY 180, AF 1410, and AerMet® 100 belong can achieve high levels of both strength and toughness through microstructural control. High strength is achieved by quenching the austenite phase to form martensite and then ageing to precipitate  $M_2C$  carbides that impede dislocation motion.  $M_2C$  carbides also help improve fracture toughness because they precipitate at the expense of  $M_3C$  carbides that reduce fracture toughness by embrittling grain boundaries.<sup>10</sup>

Three commercially important secondary hardening steels, HY 180, AF 1410, and AerMet® 100 have been awarded U.S. Patents.<sup>11,12,13</sup> Table 1 provides information on the typical mechanical properties for HY 180, AF 1410, and AerMet® 100. Tables 2a and 2b provide information on the chemistry range and typical compositions for these steels. When processed using the standard heat treatment, the hardness of AerMet® 100 is equivalent to that of 4340 with a typical fracture toughness of more than twice that of 4340.<sup>14</sup> Since the stan-

Table 1: Properties of Three Secondary Hardening Steels.

Steel	HY 180	AF 1410	AerMet® 100
US Patent Number	3,502,462	4,076,525	5,087,415
Patent Issue Date	March 24, 1970	February 28, 1978	February 11, 1992
Fracture Toughness , MPav/m (ksi/in)	203 (185)	165 (150)	132 (120)
Hardness (HRC)	43	49	53
Ultimate Tensile Strength, MPa (ksi)	1410 (205)	1725 (250)	1965 (285)
0.2% Yield Strength, MPa (ksi)	1240 (180)	1550 (225)	1725 (250)
Charpy Impact Energy, Joule (ft•lb)	81 (60)	88 (65)	40 (30)

Table 2a: Composition Ranges of Three Secondary Hardening Steels.

Element (wt%)	Steel	HY 180	AF 1410	AerMet™ 100
carbon		0.06 - 0.16	0.12 - 0.17	0.21 - 0.27
chromium		0.50 - 2.00	1.80 - 3.20	2.50 - 3.30
nickel		9.50 - 14.0	9.50 - 10.50	11.0 - 12.0
cobalt		6.00 - 10.0	11.5 - 14.5	11.0 - 14.0
molybdenum		0.70 - 1.50	0.90 - 1.35	1.00 - 1.30
iron		balance	balance	balance

Table 2b: Typical Alloy Chemistry of Three Secondary Hardening Steels.

Element (wt%)	Steel	HY 180	AF 1410	AerMet™ 100
carbon		0.1	0.16	0.24
chromium		2	2	3.1
nickel		10	10	11
cobalt		8	14	13.5
molybdenum		1	1	1.15
iron		balance	balance	balance

standard heat treatment for AerMet® 100 is not the peak hardened condition but rather an overaged condition, it should be possible to alter the heat treatment to increase hardness while retaining adequate fracture toughness for use as an armor material. As used in this thesis, "adequate" fracture toughness means equal to or greater than 55 MPa/m (50 ksi/in)—the average toughness of 4340 used for ballistic applications. The opportunity to increase hardness without compromising fracture toughness is the reason AerMet® 100 was chosen for use in this study.

#### High Yield 180

HY 180 Steel was developed for applications such as pressure vessels and submarine hulls requiring high yield strength, good notch toughness and weldability. The steel's composition permits its use both in wrought form and as a filler metal for welding. The carbon content of this steel is sufficient to promote secondary hardening but still low enough to prevent weld cracks from forming in the heat

affected zone. Speich researched the physical metallurgy of HY 180 Steel and established that strength and toughness of these steels could be simultaneously increased through dissolution of  $M_3C$  carbides and the precipitation of  $M_2C$  carbides.<sup>6</sup> This research laid the foundation for the development of AF 1410 in the mid seventies and AerMet® 100 in the late eighties.

#### Air Force 14 Cobalt - 10 Nickel (AF 1410)

AF 1410 was provides strength levels significantly greater than HY 180 while retaining high fracture toughness and corrosion resistance. Although AF 1410 has a carbon level of 0.16 wt%, welding the alloy is still possible using conventional arc welding practices. The patent for AF 1410 claims stress corrosion cracking resistance of 66 MPa/m (60 ksi/in) after 1000 hours in 3.5% sodium chloride solution. The application of vacuum processing to reduce impurity elements is essential to develop the properties listed in Table 1.

#### AerMet® 100

Carpenter Technology Corporation developed AerMet® 100 to achieve strength levels commensurate with 300M Steel while providing fracture toughness greater than 110 MPa/m (100 ksi/in). The designation "100" in AerMet® 100 stands for a fracture toughness of 100 ksi/in (110 MPa/m). The patent for AerMet® 100 specifies double vacuum processing and reduction of impurity elements to extremely low levels. In addition the presence of silicon and manganese, both of which are present in HY 180 and AF 1410 are reduced to levels less than 0.01 wt%. AerMet® 100 also includes rare earth additions such as lanthanum or cerium. The rare earth elements getter undesirable elements such as phosphorous and sulfur, thus preventing these elements from embrittling grain boundaries. The rare earth compounds also serve as a grain refining dispersion.

#### Alloying Elements

Selection of the type and quantity of alloying elements for use in secondary hardening steels has been the subject of considerable research. The following discussion identifies the primary alloying elements in HY 180, AF 1410 and AerMet® 100 Steels.

## Carbon

Carbon is responsible for hardening through carbide precipitation and interstitial solid-solution strengthening. In general, alloy strength increases with increasing carbon content, while fracture toughness decreases with increasing carbon content.<sup>15</sup> The optimum carbon addition in a secondary hardening steel is sufficient to balance the addition of carbide forming elements. Adding more carbon will have a deleterious impact on fracture toughness, while too little carbon will not result in an optimal combination of strength and toughness.

## Nickel

Nickel has three primary effects on precipitation hardening steels. As a substitutional element, nickel promotes increased hardness through the formation of a lath martensitic microstructure. Nickel lowers the  $M_s$  temperature, thereby increasing the amount of retained austenite. Nickel also lowers the nil ductility temperature, resulting in ductile fracture at room temperature, even for high strength levels.<sup>15</sup>

## Cobalt

Cobalt increases the  $M_s$  temperature, refines the martensitic structure, and promotes retention of the dislocation substructure at higher tempering temperatures. The higher dislocation density is important because more sites are available for carbide precipitation, resulting in a finer distribution of precipitates. The combination of cobalt and nickel provides the basis for exploitation of precipitation hardening in these steels. Without nickel, this class of alloy would not have adequate toughness. Without cobalt, the high nickel content would lead to unacceptable levels of retained austenite on quenching.

## Molybdenum

Molybdenum is a strong carbide former and helps increase peak hardness. The strength increase results from the formation of  $Mo_2C$  in the steel. Molybdenum is always added to secondary hardening steels in combination with chromium. Without the addition of molybdenum little or no secondary hardening takes place.

### Chromium

Although chromium also forms alloy carbides, in the presence of molybdenum, chromium goes into solution in the Mo<sub>2</sub>C carbide. Chromium also shifts the secondary hardening peak to lower temperatures and to higher hardness values than would be possible with only molybdenum additions.<sup>3</sup>

### Rare Earth Additions

Rare earth elements such as lanthanum and cerium are added to AF 1410 and AerMet® 100 to form compounds with impurity elements. The Group VI elements such as phosphorous and sulfur have a particularly deleterious effect on grain boundary cohesion even at concentrations below 100 parts per million (ppm).<sup>16</sup> Lanthanum and cerium are usually selected to getter impurity elements because they have the lowest free energy of formation.<sup>17</sup> Compounds of rare earth and impurity elements can also provide a grain refining dispersion that is stable at solution treatment temperatures approaching 1110°C (1850°F).<sup>17</sup>

### Stress Corrosion Cracking

The use of ultrahigh strength steels in demanding structural applications is often accompanied by service failures attributed to stress corrosion cracking. The mechanism associated with these failures is hydrogen embrittlement, defined in this thesis as cathodic charging at a crack or other flaw. Aircraft components such as pitch links, main rotor retention nut, and mixer pivot support have been the subjects of failure analyses.<sup>18,19,20</sup> These in-service failures are a primary motivation for the ongoing development of ultrahigh strength steels with high fracture toughness. As higher levels of fracture toughness are realized, the critical flaw size to produce failure in ultrahigh strength steel components is increased. Additionally, slower crack growth rates are generally associated with higher toughness steel, so that inspection intervals can be extended or inspection reliability improved. For these reasons, analysis of stress corrosion cracking resistance should accompany development of a new ultrahigh strength steel.

Unlike most mechanical property tests, there is no standardized procedure to measure the threshold stress intensity for stress corrosion cracking of metallic materials. ASTM Committee E-24 is presently developing a standard for deter-

mining the threshold stress intensity factor for environment-assisted cracking of metallic materials under constant load. In its current form, the draft standard relies heavily on existing techniques for plane-strain fracture toughness testing and a substantial body of literature on stress corrosion cracking dating to the 1960s.

Brown introduced the concept of threshold stress intensity factor for stress corrosion cracking using precracked cantilever beam tests.<sup>21</sup> The threshold stress intensity for stress corrosion cracking of a particular material-environment system, denoted  $K_{ISCC}$ , is the stress intensity below which subcritical crack extension does not occur under a static load. The three prerequisites for stress corrosion cracking are: 1) an aggressive environment; 2) a susceptible material; 3) an applied load. Although the cantilever beam test has been used widely to determine  $K_{ISCC}$  values for numerous materials, the absence of a governing standard has been problematic.

For example, no two laboratories use precisely the same test fixture to perform their experiments. Moreover, different specimen geometries have resulted in different time to failure curves for the same material tested at different facilities. One of the difficulties in establishing a value for  $K_{ISCC}$  under these conditions is determining how long to wait before terminating a test. As will be shown later in this thesis, the selection of an arbitrary test duration time such as 1000 hours can lead to significant overstatement of the actual value for  $K_{ISCC}$ .

### **3.0 Research Program**

The research program described in this thesis was established to determine relationships between the processing, microstructure, and properties of AerMet® 100 Steel. The primary objective was to determine the maximum hardness capability of AerMet® 100 and then proceed to determine the alloy's ballistic and mechanical properties when peak hardened. The processing variables considered in this study include solution treatment temperature, quenching parameters, cryogenic treatment, and ageing treatments. Earlier work on the physical metallurgy of the family of steels to which AerMet® 100 belongs established the morphology of the particles responsible for secondary hardening.<sup>6,22</sup> The properties evaluated for this study include strength, fracture toughness, impact energy, stress corrosion cracking resistance, and ballistic tolerance.

The experimental approach involved development of processing curves showing hardness as a function of solution treatment temperatures and hardness as a function of time for two ageing temperatures. Hardness was the variable selected for optimization because it generally correlates with ballistic performance. On the basis of mechanical property data and knowledge of AerMet® 100's physical metallurgy, four heat treatments for ballistic plates were selected. Coupled with published data on shear instability, the results of ballistic testing provide information on the influence of small scale microstructural features on high strain rate phenomena and their underlying deformation mechanisms.<sup>23</sup> Stress corrosion cracking tests were also conducted in 3.5 wt% sodium chloride solution to determine AerMet® 100's susceptibility to an aggressive environment.

## **4.0 Experimental Procedures**

### Material and Processing

The Materials Directorate of the U.S. Army Research Laboratory (ARL-MD) purchased the AerMet® 100 alloy (bar stock and plates) used for this study from Carpenter Technology Corporation (CarTec).<sup>24</sup> CarTec supplied ARL-MD with material from Heat Number 89557. Chemical analysis of Heat 89557 is displayed in Table 3. Table 4 shows the chemical composition required by Aerospace Material Specification (AMS) 6532. Comparison of the AMS requirements with the material used for this study indicate that Heat 89557 was of high pedigree.

The alloy was double vacuum melted, first as a 61 cm (24 inch) diameter vacuum induction melted (VIM) electrode, second as a 76 cm (30 inch) diameter vacuum arc remelted (VAR) ingot. Before VAR, electrodes were stress relieved at 677°C (1250°F) for 4 to 16 hours and air cooled. After VAR, the material was homogenized at 2150°F for 6 to 10 hours. The ingot was bloomed to a cross section of 12.7 cm by 127 cm (5 inch by 50 inch) and the plate was cross-rolled to final thickness. After rolling, CarTec overage-annealed the plates at 677°C (1250°F) for 16 hours to a hardness of 39 Rockwell C (HRC). Samples measuring 30.5 cm (12 inches) square were then cut from the plates. The mechanical properties certified by CarTec are included in Table 5. All of the certified properties match typical values for the alloy with the exception of ultimate tensile strength, which is approximately 70 MPa (10 ksi) lower than expected.

### Development of Ageing Curves

The first experimental task was to identify heat treatment parameters including solution (austenitizing) temperature, ageing time, and ageing temperature. For

Table 3: Chemical Analysis of AerMet® 100 Heat 89557 by Weight Percent.

C	0.24	P	0.003	Al	0.009
Co	13.4	S	0.001	O	< 0.001
Ni	11.07	Mn	0.01	N	< 0.001
Cr	3.09	Si	0.01	P + S	0.004
Mo	1.17	Tl	0.012		

Table 4: AerMet® 100 Chemistry Requirements from AMS Specification 6532.

C	0.21 - 0.25	P (max.)	0.008	Al (max.)	0.015
Co	13 - 14	S (max.)	0.005	O	< 0.002
Ni	11 - 12	Mn (max.)	0.1	N	< 0.015
Cr	2.9 - 3.3	Si (max.)	0.1	P + S (max.)	0.01
Mo	1.1 - 1.3	Ti (max.)	0.015		

Table 5: Manufacturer's Certified Properties for Heat 89557.

Yield Strength (0.20%)	1745 MPa (253 ksi)
Tensile Strength	1900 MPa (276 ksi)
Elongation	13% in 5.1 cm (2 inch)
Hardness	52 HRC

the solution treatment and ageing treatment studies, we sectioned pieces measuring approximately 1.3 cm (0.5 inch) cubed from the bar stock measuring 12.7 cm wide by 5.1 cm tall by 46 cm long (5 inches by 2 inches by 18 inches). The orientation of each cube relative to the parent stock was marked on each face.

The specimens used for the solution treatment study were all heat treated in air for one hour at temperatures ranging from 830°C (1525°F) to 1080°C (1975°F) and air cooled. Upon arrival at room temperature, the specimens were cut in half using a Buehler Isocut Plus cutoff saw equipped with a type 11-4207 blade rotating at 3500 rpm under an applied load of 250 grams with circulating coolant. After sectioning, the outside face opposite the cut face was ground to remove decarburization and scale. Rockwell C measurements were then taken on the cut face of each specimen according to American Society for Testing and Materials (ASTM) Standard E-18.<sup>25</sup> At least eight measurements were taken on each specimen. These data provided the one hour solution treatment temperature that produced the maximum as-cooled hardness.

Next, we determined the ageing response for two ageing temperatures for times ranging from one minute to sixteen hours. All of the ageing specimens were first solution treated based on the results of the solution treatment study. The same specimen preparation and measurement techniques used for the solution treatment study were also used for the ageing study. For ageing times less than thirty minutes, specimens were aged in molten lead to ensure proper control over ageing time. The typical temperature deviation in the lead pot was  $\pm 1.7^{\circ}\text{C}$  ( $\pm 3^{\circ}\text{F}$ ). Specimens aged for thirty minutes and longer were heated in a conventional laboratory furnace with a maximum deviation of  $\pm 6^{\circ}\text{C}$  ( $\pm 10^{\circ}\text{F}$ ). The surface temperature of each specimen was monitored with a thermocouple during ageing.

The temperatures selected for the ageing experiments were based on recently published data. Novotny studied heat treatment response of AerMet® 100 over a very broad range of solution treatments and ageing temperatures.<sup>26</sup> His study focused on ageing times of 1, 3, 5 and 8 hours at various temperatures after a solution treatment temperature of  $885^{\circ}\text{C}$  ( $1625^{\circ}\text{F}$ ). Whereas Novotny's study dealt with a broad range of solution treatment temperatures and tended to favor examination of overaged microstructures this study focused on detailed examination of a narrower range of time-temperature combinations so that a material condition with the best combination of hardness, fracture toughness, and ballistic performance could be selected.

#### Short Range Order Experiment

Schmidt and Gore reported that post ageing treatments applied to AF 1410 steel produced a hardness increase of over 20 DPH (Diamond Pyramid Hardness).<sup>27</sup> They attributed the observed behavior to possible short range ordering. The time required for this hardness increase was between five and thirty hours. Short range ordering is expected to manifest itself by an incremental increase in hardness and a corresponding increase in tensile properties.

To determine if AerMet® 100 displayed similar behavior, a post age treatment was conducted at  $370^{\circ}\text{C}$  ( $700^{\circ}\text{F}$ ) on hardness and tensile specimens to determine any variations in both hardness and tensile property data as a function of time. Prior to the post age treatment, all specimens were heat treated using

the standard practice of 885°C (1625°F), one hour, air cool; -73°C (-100°F), one hour, air warm; 482°C (900°F), five hours, air cool. Both Rockwell C and Vickers Hardness tests were performed on the same type of specimen used for the solution treatment and ageing studies. Vickers Hardness Tests were conducted according to ASTM Standard E-92.<sup>29</sup>

### Mechanical Properties

Mechanical property tests were conducted to determine the strength, fracture toughness and Charpy impact energy for four different heat treatments. Longitudinal tensile tests were conducted according to ASTM Standard E-8.<sup>29</sup> Fracture Toughness tests were conducted according to ASTM Standard E-399 on specimens machined in the L-T orientation.<sup>30</sup> Longitudinal Charpy impact energy was measured according to ASTM Standard E-23.<sup>31</sup> At least two specimens were used for each test and material condition evaluated.

### Stress Corrosion Cracking Tests

All of the stress corrosion cracking specimens were solution treated at 885°C (1625°F) for one hour and oil quenched. Upon reaching room temperature, all the specimens were placed in a cryogenic bath at -73°C (-100°F) and held for one hour. The specimens were then divided into two groups. The first group was aged at 482°C (900°F) for five hours; the second group, at 468°C (875°F) for five hours. The first ageing treatment is the standard condition recommended by Carpenter Technology. The second treatment is of interest because commercial airline manufacturers and the Department of Defense (DoD) have expressed interest in a higher strength version of AerMet® 100.

A specimen geometry and experimental apparatus were selected to permit comparison to data developed at the Naval Air Warfare Center (NAWC) in Warminster, PA.<sup>32</sup> The environment selected consisted of 3.5 wt% sodium chloride (NaCl) in water. This environment has the same nominal sodium chloride concentration as seawater and was also used by NAWC for their experiments.

The specimens were machined in the L-T orientation, such that the crack is coincident with the transverse direction of the parent stock. The specimen's dimensions after final machining were 2.54 cm high by 1.27 cm wide by 17.8

cm long (1 inch by 0.5 inch by 7 inches). A notch measuring 0.191 cm (0.075 inch) deep with a maximum root radius of 0.01 cm (0.004 inch) and included angle of 45° was machined into the specimen. A diagram of the specimen is shown in Figure 1. Each specimen was precracked approximately 0.127 cm (0.050 inch), so that the total flaw size (notch + precrack) was approximately 0.318 (0.125 inch).

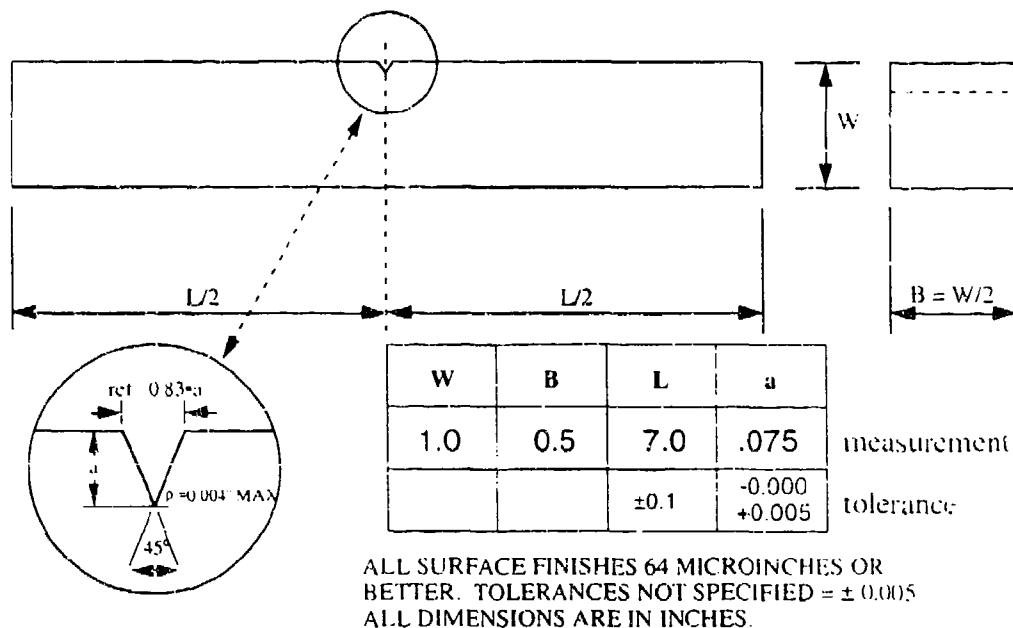


Figure 1: Cantilever Beam Specimen Used for Stress Corrosion Cracking Tests.

This geometry associated with this initial flaw size does not comply with ASTM E-399, which specifies an initial flaw size ( $a$ ) to specimen depth ( $W$ ) ratio of  $0.45 < a/W < 0.55$ . Few laboratories seem to use this geometrical requirement for stress corrosion cracking tests. The NAWC tests on AerMet® 100 were conducted using an  $a/W$  ratio of 0.125. Other investigations such as those of Beachem and Brown used values of  $a/W = 0.35$ .<sup>33</sup> While the  $a/W$  ratio required by E-399 is appropriate for plain strain fracture toughness testing in air, it need not be applied to stress corrosion cracking tests.

The crack length must be chosen in conjunction with the specimen thickness, taking plastic zone size effects into consideration.<sup>34</sup> The selection of

$0.45 < a/W < 0.55$  for plane strain fracture toughness testing is derived from this rationale.<sup>35</sup> For stress corrosion cracking tests, the applied stress intensity is significantly less (~20% of  $K_{IC}$ ) than for a fracture toughness test in air. As a result, it is possible to use a shorter initial flaw size provided the flaw size exceeds  $2.5 \cdot (K/\sigma_y)^2$ , as recommended by ASTM STP 410.<sup>36</sup> For an applied  $K$  of 55 MPa $\sqrt{m}$  (50 ksi $\sqrt{in}$ ) and  $\sigma_y = 1795$  MPa (260 ksi) for AerMet® 100, the minimum flaw size would be 0.235 cm (0.0925 inch). Since this value is less than the 0.318 cm (0.125 inch) flaw size used for the NAWC tests, it seems acceptable to use a short flaw size ( $a/W > 0.0925$ ) for the stress corrosion cracking tests. The important fact to remember is that identifying the stress intensity resulting in sub-critical crack growth is the primary objective of the stress corrosion cracking test. By the time the crack has grown to critical length, the geometry is more akin to that required by ASTM E-399.

The notched region of the specimen was surrounded by a polyethylene cell containing approximately 250 ml of the sodium chloride solution (pH 5.5 - 6.0).

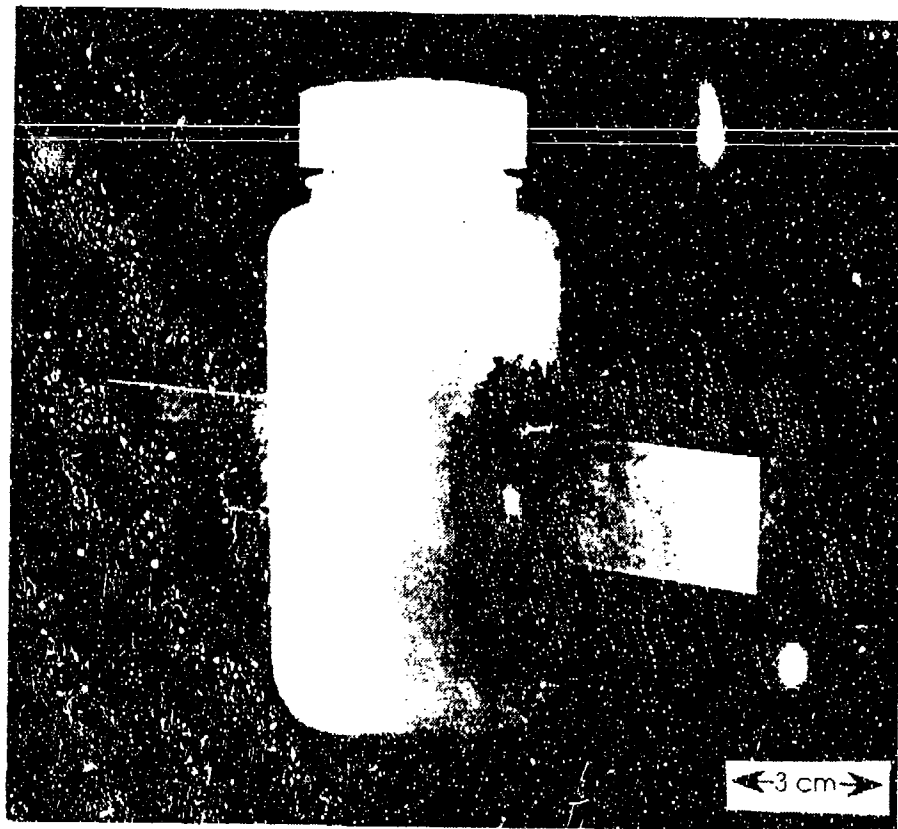


Figure 2: Cantilever Beam Specimen Mounted in Corrosion Cell.

Dow Corning sealant 3145 RTV, a silicone rubber adhesive and sealant free from solvents that might influence the test results, was used to seal the area where the polyethylene cell contacts the specimen. The solution was prepared with reagent grade sodium chloride and distilled water. Once the test began, the solution was changed once every week. A photograph of a cantilever beam specimen mounted in the polyethylene cell is shown in Figure 2.

Values for the initial stress intensity were selected to produce failure times ranging from a few hundred hours to more than 1000 hours. The Kies equation was used to determine the weight required to produce the desired stress intensity:<sup>37</sup>

$$K_I = \frac{4.12 \cdot M \cdot \sqrt{\frac{1}{\alpha^3} - \alpha^3}}{B \cdot W^{3/2}} \quad (2)$$

where: B = Specimen Thickness

W = Specimen Depth

M = The Applied Bending Moment at the Crack Tip

$\alpha$  = the initial flaw size

$$\alpha = a - \frac{a}{W}$$

Figure 3 shows a schematic physical description of the cantilever beam equipment used for our experiments. A photograph of an actual cantilever beam fixture is displayed in Figure 4a, with a close up of the specimen shown in Figure 4b.

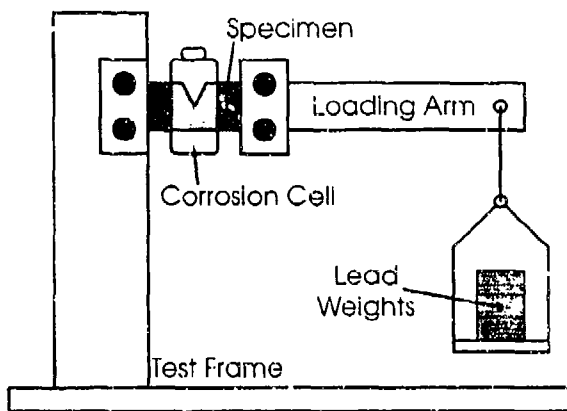


Figure 3: Schematic of Cantilever Beam Apparatus.

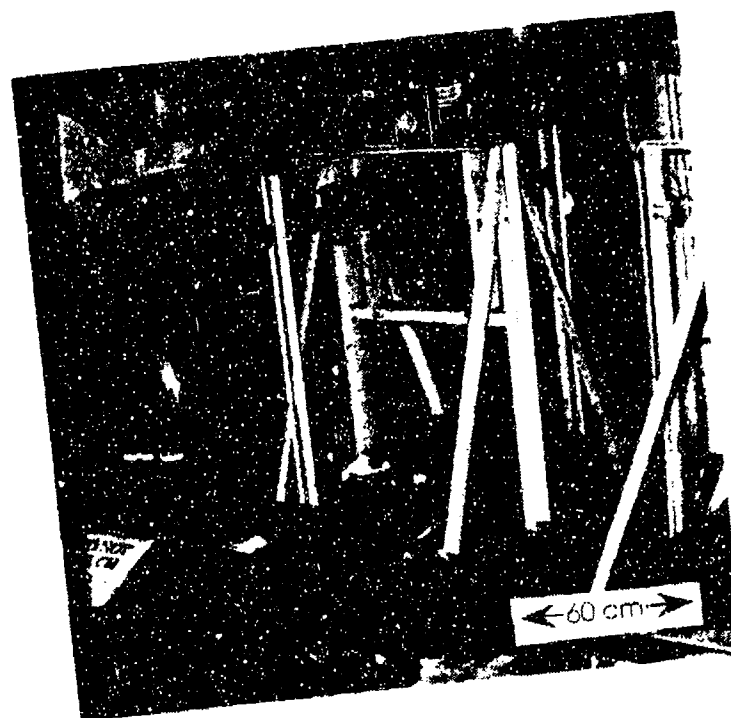


Figure 4a: Cantilever Beam Apparatus.

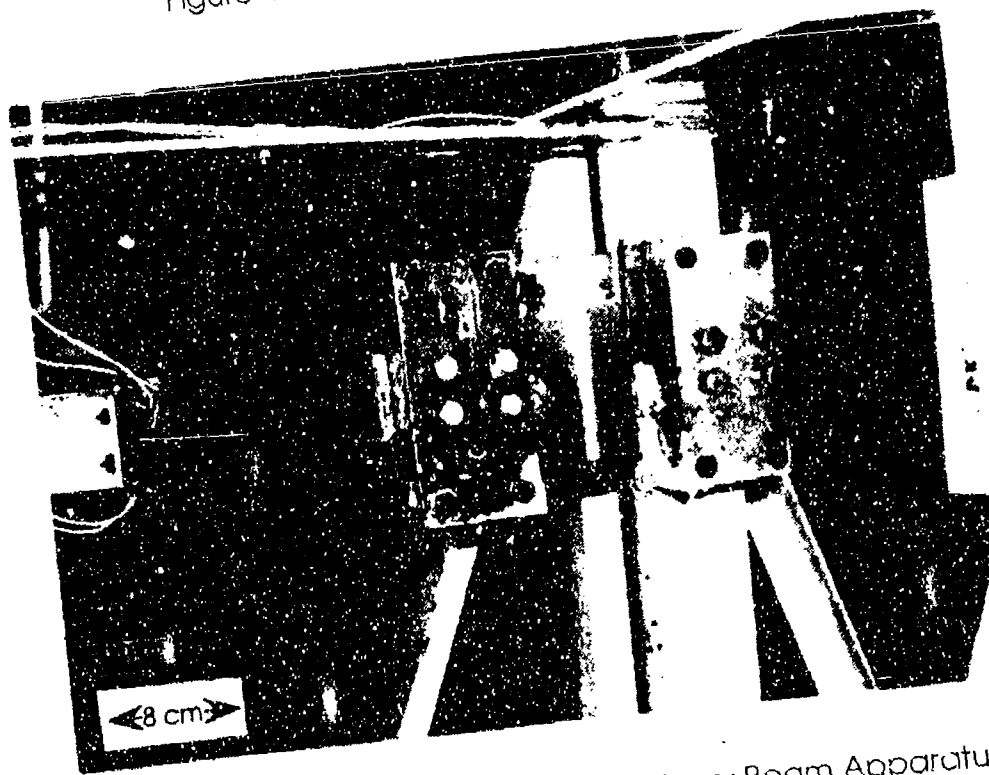


Figure 4b: Specimen Mounted in Cantilever Beam Apparatus.

### Processing of Ballistic Plate

On the basis of results from the solution treatment study, all of the plates were solution treated together at 885°C (1625°F) for one hour at temperature in an L&L specialty furnace equipped with a recirculator using a flowing argon atmosphere. Although it does not produce a completely neutral atmosphere, the argon atmosphere minimizes scale and decarburization. Results from the ageing study were used to select four different ageing treatments. One of the ageing treatments—five hours at 482°C (900°F)—is recommended by CarTec. Another treatment—five hours at 468°C (875°F)—was selected because CarTec has applied for an AMS specification using this time-temperature combination. Since the objective was to produce the hardest material possible, the final two ageing treatments—one hour at 468°C (875°F) and one hour at 482°C (900°F)—were selected to produce peak hardness of 55 HRC to 56 HRC.

After heat treatment, the plates were ground on a Blanchard grinder using a 36 - 40 grit alumina wheel and a soluble oil coolant to remove the decarburized layer and scale that often influence the results of ballistic testing. First, the plates were ground to produce parallel surfaces to within 0.038 cm (0.015 inch), and then further ground to remove at least 0.051 cm (0.020 inch) from the impact face to ensure complete removal of the decarburized layer. This surface preparation technique inherently produces machining marks on the plate surface.

### Ballistic Tests

Ballistic tests were conducted according to MIL-STD-662E, *V<sub>50</sub> Ballistic Test for Armor*.<sup>38</sup> Two different small arms projectiles were selected for ballistic testing: the U.S. 0.30 caliber (7.62 mm) armor piercing (AP) M2 and the U.S. 0.50 caliber (12.7 mm) AP M2. The 30.5 cm (12 inch) square ballistic test plates were mounted to a test fixture by clamping each corner with a C clamp. The ballistic test fixture consisted of a steel frame with an opening measuring 25 cm (10 inches) square. A sheet of 0.051 cm (0.020 inch) thick 2024-T3 aluminum alloy termed a 'witness plate' or 'witness sheet' was placed 15 cm (6 inches) behind the target to indicate any spall or residual projectile fragments emanating from the rear face of the target during ballistic impact.

The final condition of the witness plate determines the outcome of the ballistic test. If the witness plate is perforated by the projectile or spall from the test panel, the result is recorded as a complete penetration. If no perforation is observed through the witness plate, the result is recorded as a partial penetration. Note that if the test panel is perforated but the witness plate remains intact, the result is a partial penetration. A schematic definition of partial and complete penetrations is shown in Figure 5.

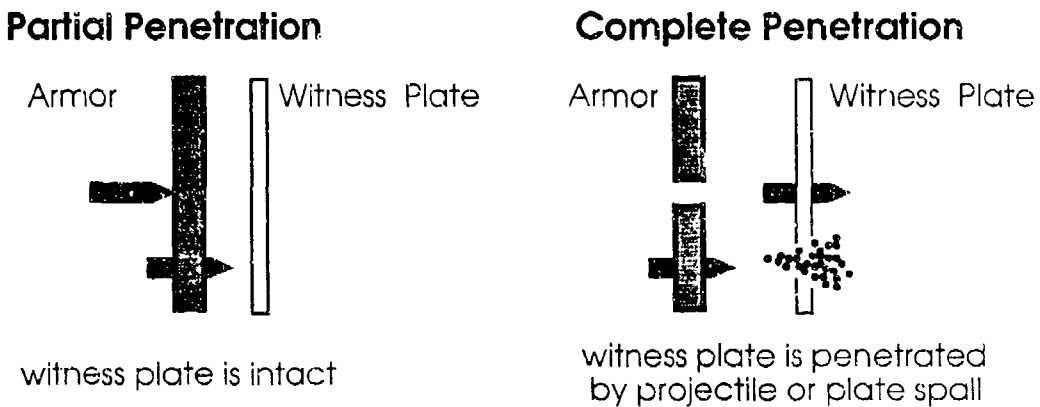


Figure 5: Definition of Partial and Complete Penetration.

Projectiles were fired from a barrel mounted to a rigid support. Projectile velocity was determined using paper break screens separated by a known distance and time counters that recorded the time lapse to the nearest microsecond. The paper break screens are coated with a connected pattern of silver paint lines. When the screen is intact, the resistance from one side to the opposite side is essentially zero; when the screen is perforated, the resistance becomes infinite. As the projectile travels downrange, it strikes the first paper screen, initiating a timing device. The timer counts until the second paper screen is broken. The projectile velocity is equal to the elapsed time divided by the distance between the two break screens.

For the 0.50 caliber (12.7 mm) tests a Browning barrel was used. The barrel muzzle end was 6.1 m (twenty feet) from the target. The distance between velocity screens was 3.05 m (ten feet).

For the 0.30 caliber (7.62 mm) tests, a standard service barrel was used. The barrel muzzle end was 6.1 m (ten feet) from the target. The distance between velocity screens was 61 cm (two feet). The same timing mechanism was used for both the 0.50 caliber (12.7 mm) and 0.30 caliber (7.62 mm) tests.

## 5.0 Experimental Results

### Solution Treatment

Results from the solution treatment experiment are shown in Figure 6. The peak as cooled hardness of 50.8 HRC was found for a solution treatment temperature of 885°C (1625°F). Carpenter Technology recommends this temperature for solution treatment of AerMet® 100 and it is also the solution temperature used by Novotny. On the basis of these solution treatment results, we selected a solution treatment temperature of 885°C (1625°F) for use throughout the remainder of this thesis.

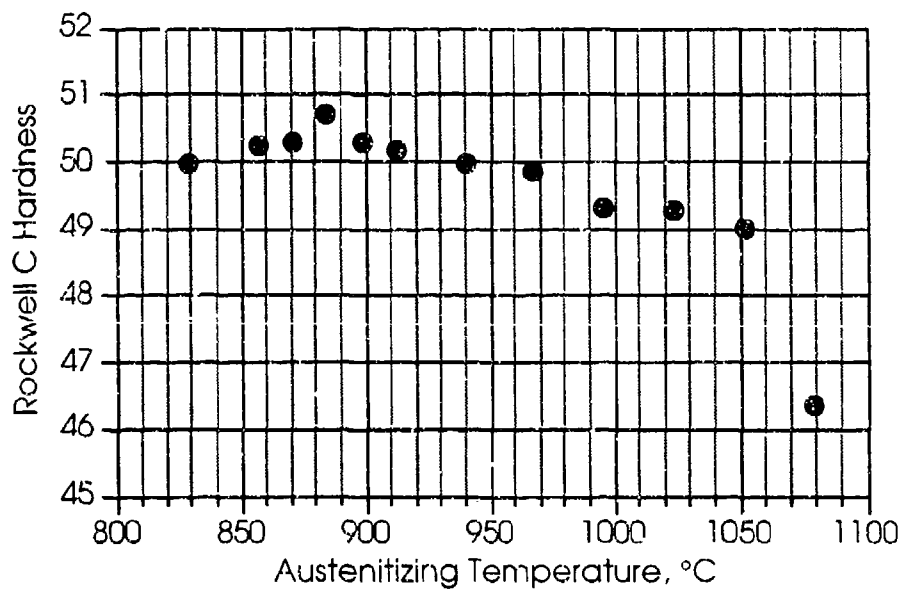


Figure 6: Effect of Solution Treatment Temperature on the As Cooled Hardness of AerMet® 100.

### Ageing Study

Several factors influenced our selection of the two ageing temperatures. At temperatures in excess of 482°C (900°F), the austenite content in the microstructure increases, leading to reduced hardness.<sup>26</sup> Below 468°C (875°F), significant M<sub>3</sub>C in the microstructure adversely affects the steel's toughness. Although M<sub>2</sub>C can precipitate below 468°C (875°F), the resultant kinetics do not allow the development of adequate toughness after a five hour age.

Table 6: Heat Treatments Selected for Ballistic Plates.

Temperature	Time	Hardness (HRC)	Microstructure
482°C (900°F)	5 hours	52 - 53	overaged
482°C (900°F)	1 hour	55.5 - 56	peak aged
468°C (875°F)	5 hours	53	slightly overaged
468°C (875°F)	1 hour	54	slightly underaged

A graph of results from the ageing experiments at 468°C (875°F) and 482°C (900°F) is shown in Figure 7. Average peak hardness of 55.5 HRC was obtained for a one hour age at 482°C (900°F). For the 468°C (875°F) age, average peak hardness of 55.2 HRC was obtained for an ageing time of three hours. However, because the resolution of the Rockwell C hardness test is, at best, 0.5 points, it is more accurate to place the peak ageing time for 468°C (875°F) between one and three hours.

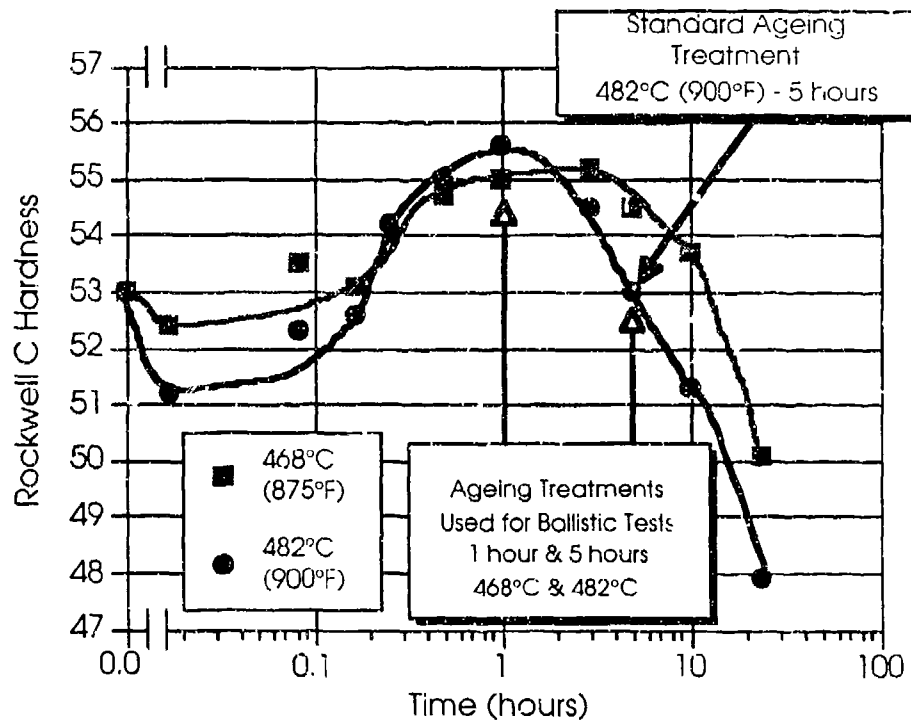


Figure 7: Results of AerMet® 100 Ageing Study.

The results of the ageing study were used to select four ageing treatments for the ballistic plate material. Table 6 shows a summary of the treatments we selected, the average hardness measured on the surface of the plates, and the anticipated microstructure. Microhardness measurements on corner sections taken from each plate indicated that significant decarburization was limited to between 0.025 cm (0.010 inch) and 0.051 cm (0.020 inch) below the surface. The measured hardness values are somewhat lower than anticipated based on the data shown in Figure 7. These lower hardness values may have resulted from the surface preparation technique applied to the plates.

#### Short Range Order Experiment

The results of the short range order experiments are graphed in Figure 8. Although an increase in Vickers (Diamond Pyramid, DPH) Hardness of between

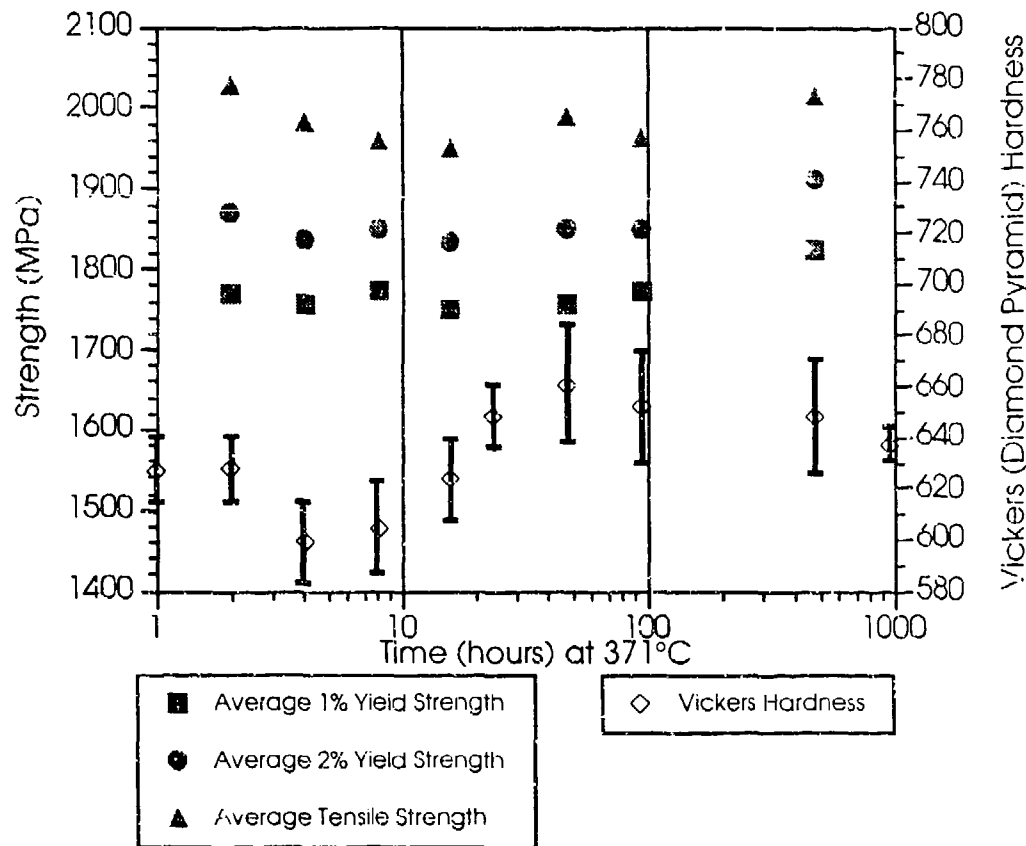


Figure 8: Hardness and Strength as a Function of Ageing Time for a Two Step 482°C (900°F) five hour, 371°C (700°F) Ageing Treatment.

20 and 40 points was observed, tensile properties showed no dramatic influence from the post age treatment. Rockwell C Hardness (HRC) measurements (not shown) were also taken and showed no discernible change in hardness level as a function of ageing time. Because the DPH test is much finer in scale than the HRC test, the variation in DPH measurements are more likely related to local microstructural differences.

Table 7: Measured Mechanical Properties of AerMet® 100 Steel.

Temperature Time	900°F 5 hours	875°F 5 hours	900°F 1 hour	875°F 1 hour
Hardness (HRC)	53	54	55.5	55
Ultimate Tensile Strength, MPa (ksi)	1966 (285)	2097 (304)	2145 (311)	2131 (309)
0.2% Offset Yield Strength, MPa (ksi)	1793 (260)	1876 (272)	1834 (266)	1766 (256)
Yield/Tensile Ratio	0.91	0.89	0.85	0.83
% Reduction in Area	65	58	58	56
% Elongation	15.5	13.2	14	15.5
Elastic Modulus, GPa (psi x 10 <sup>6</sup> )	175 (25.4)	192 (27.9)	179 (25.9)	188 (27.3)
Fracture Toughness, MPa√m (ksi√in)	125 (114)	94 (86)	89 (81)	71 (65)
Charpy Impact Energy, Joules (ft•lb)	41 (30.3)	33 (24.5)	29 (21.3)	28 (20.8)

### Mechanical Properties

Mechanical property data are displayed in Table 7. The results for the 482°C (900°F) and 468°C (875°F) five hour ages compare most favorably with CarTec's published data for AerMet® 100 and indicate that heat treatment procedures used in this study were consistent with applicable processing specifications.

During analysis of fracture surfaces with a scanning electron microscope (SEM), several particles bearing cerium and phosphorous were identified. Although CarTec does not publish all details related to the processing of AerMet® 100, this finding indicates rare earth modification (REM) probably by late addition of a cerium bearing compound during vacuum induction melting.

### Stress Corrosion Cracking Tests

Data obtained from the cantilever beam stress corrosion cracking tests are graphed in Figure 9. The 482°C (900°F) specimen loaded to an initial stress intensity of 38 MPa/m (35 ksi/in) developed a bifurcated crack and failed after 1200 hours. The plot shows the initial stress intensity factor plotted as a function of time to failure for each of the two aging treatments. Comparative data from a study by Kozol and Neu for specimen's aged five hours at 482°C (900°F) are included.<sup>39</sup> Kozol and Neu used L-T specimens with the precrack coincident with the transverse direction of the parent stock for their tests, the same type of specimens used in this study. The slightly longer times to failure recorded during the Navy's testing may indicate a slightly different environment. Alternatively, the difference could be related to slightly different test fixturing as mentioned in the beginning of the thesis.

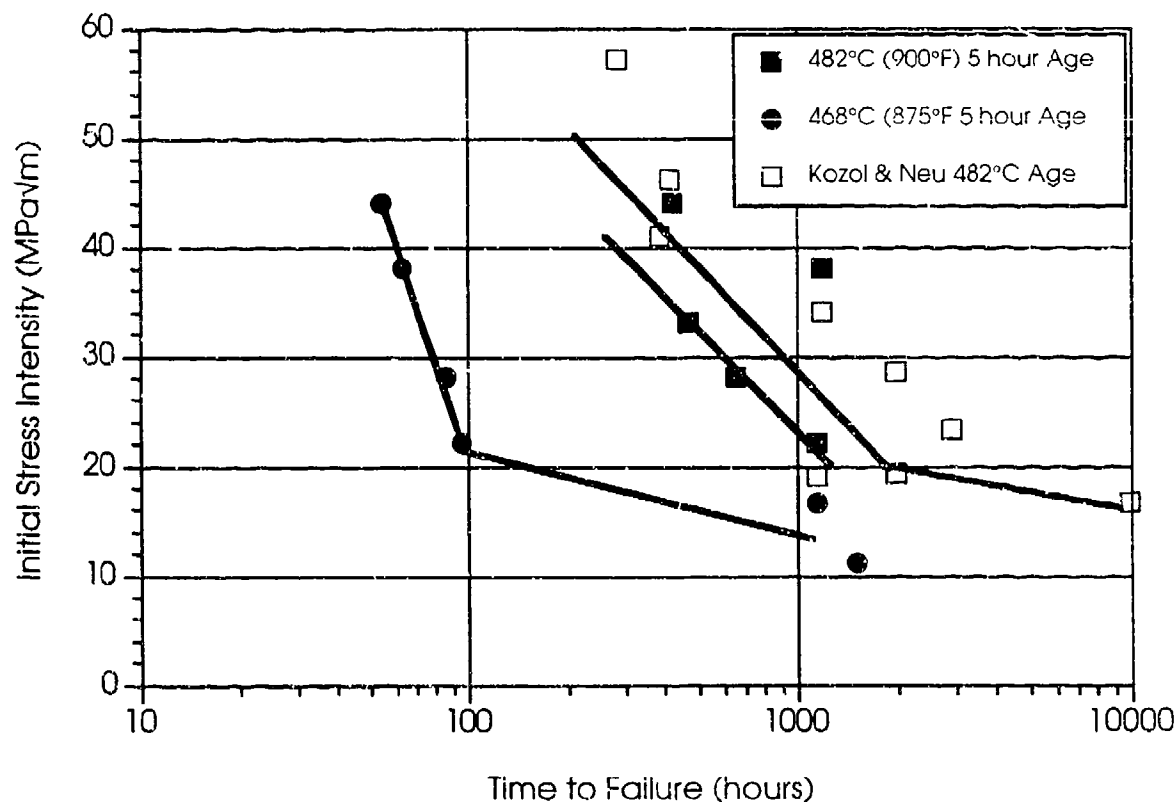


Figure 9: Results of Cantilever Beam Stress Corrosion Cracking Tests.

Using the time to failure data, we can develop a rough estimate of the crack growth velocity by dividing the distance the crack grew by the time to failure. Although this calculation is crude, it is not unreasonable since we are in a regime of crack growth where  $da/dt$  does not vary strongly with stress intensity.

#### Ballistic Tests

Results from ballistic tests of AerMet® 100 versus the 0.30 caliber (7.62 mm) AP M2 projectile are displayed in Figure 10. This graph shows the  $V_{50}$  Protection Ballistic Limit (PBL) plotted as a function of areal density. The areal density is equal to the target weight divided by the target's surface area. The numbers adjacent to each symbol indicate the number of test firings used to calculate the  $V_{50}$  PBL. For example, '5 & 5' indicates that velocities from five complete penetrations and five partial penetrations were used to calculate the  $V_{50}$ . These data show that plates heat treated at peak and near peak hardness have a  $V_{50}$  PBL approximately 120 meters per second (mps) (400 feet per second, fps) greater than the plates processed using the standard heat treatment. All of the plates showed excellent multiple hit capability. In two cases, more than twenty-five rounds were fired at a single target.

Results for AerMet® 100 versus the 0.50 caliber (12.7 mm) armor piercing M2 projectile are shown in Figure 11. During these tests, two of the peak aged plates showed a tendency to crack during ballistic impact. These cracks typically emanated on or near the impact hole and were coincident with machining marks on the surface of the plate.

Although some of the peak hardened plates were found to have higher  $V_{50}$  velocities than the 482°C (900°F) five hour age baseline plates, the increase was not as dramatic as found for the 0.30 caliber (7.62 mm) threat. For all but the 482°C (900°F) one hour plate that shattered, the increase was usually within the scatter accepted for a  $V_{50}$  PBL Test—approximately 30 mps (100 fps). Photographs of the front and rear face of each ballistic plate are displayed in Appendix A.

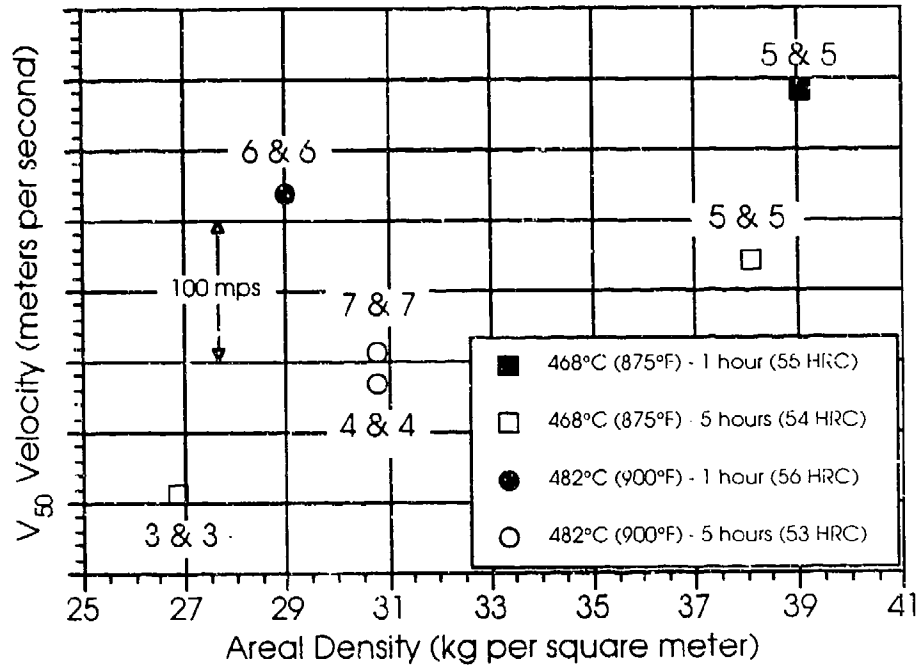


Figure 10: Results of 0.30 Caliber AP M2 Ballistic Tests on AerMet® 100 Steel.

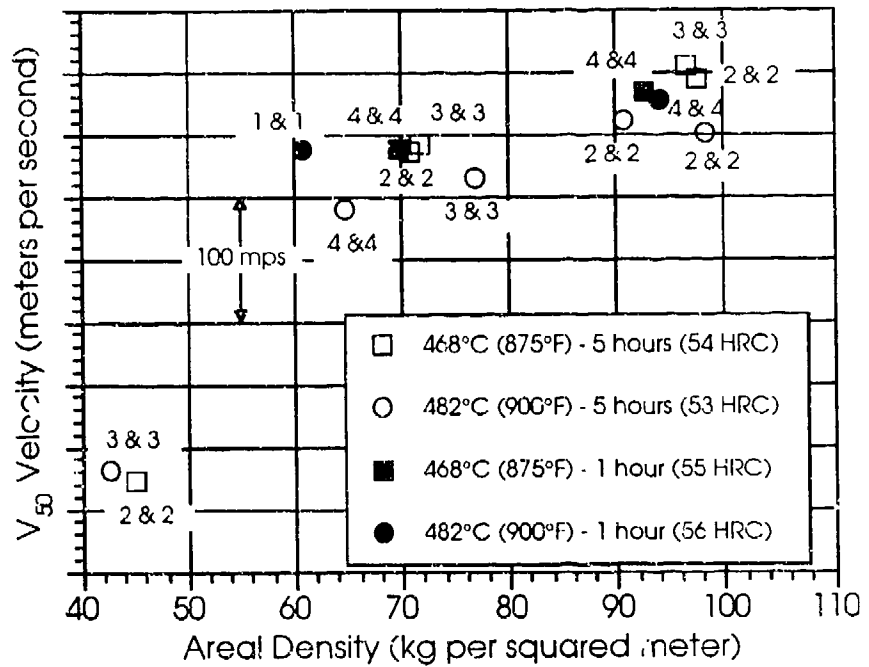


Figure 11: Results of 0.50 Caliber AP M2 Ballistic Tests on AerMet® 100 Steel.

## **6.0 Discussion**

### Processing and Properties

Prior studies on the heat treatment of AerMet® 100 by Novotny and AF 1410 by Montgomery indicate that the 482°C (900°F) treatment produces overaged M<sub>2</sub>C carbides in the microstructure, while the 468°C (875°F) five hour age produces slightly overaged M<sub>2</sub>C carbides in a microstructure retaining some M<sub>3</sub>C carbides.<sup>22,26</sup> Thus, from these studies and the hardness data presented in Figure 7, the microstructures corresponding to the peak hardened condition probably consist of mixed' M<sub>2</sub>C and M<sub>3</sub>C carbides for the one hour age at 482°C (900°F) and M<sub>3</sub>C carbides with M<sub>2</sub>C nuclei for the one hour age at 468°C (875°F).

### Ballistic Tests

The ballistic performance of AerMet® 100 aged at 482°C (900°F) for five hours is at least as good as that of 4340 steel heat treated to a hardness of between 52 and 53 HRC. The superior multiple hit capability of AerMet® 100 is probably related to fracture toughness, where AerMet® 100 steel has a fracture toughness twice that of 4340 steel.

The use of alternate heat treatments to increase the hardness of AerMet® 100 Steel provided exceptional results for one of the two small arms projectiles used for this thesis. If the improvement in ballistic performance were due exclusively to the increased hardness, one would expect all of the higher hardness plates to have higher V<sub>50</sub> velocities, regardless of their thickness. Since this is not the case, hardness is not the only variable responsible for improved ballistic performance. It may be that the thinner plates tested versus the 0.30 caliber (7.62 mm) threat were in a different stress state than the thicker plates tested versus the 0.50 caliber (12.7 mm) threat. The 0.30 caliber (7.62 mm) plates required more grinding to produce parallel surfaces. This explanation has some analogy to fracture toughness, which increases under conditions other than plane strain.

Beatty measured the shear instability strain of AerMet® 100 heat treated to the same specifications as the plates used for ballistic tests.<sup>23</sup> He performed quasi-static tests using a double-linear shear specimen to determine the shear instability strain,  $\gamma_i$ , defined as the maximum uniform strain achieved in shear before

gross localization of the strain occurs. The sample design and test have been described in detail previously.<sup>40,41</sup>

The results from these shear instability tests are shown in Figures 12 and 13. Figure 12 compares the different AerMet® 100 microstructures (heat treatments), including the type of product—plate stock or extruded stock. Figure 13 compares the shear instability strain of AerMet® 100 to a number of other high strength steels. While AerMet® 100 shows superior resistance to unstable shear compared to many high strength steels, these results demonstrate the sensitivity ( $\gamma_i$  ranges between 0.4 and 1.6) of this alloy to the treatments studied.

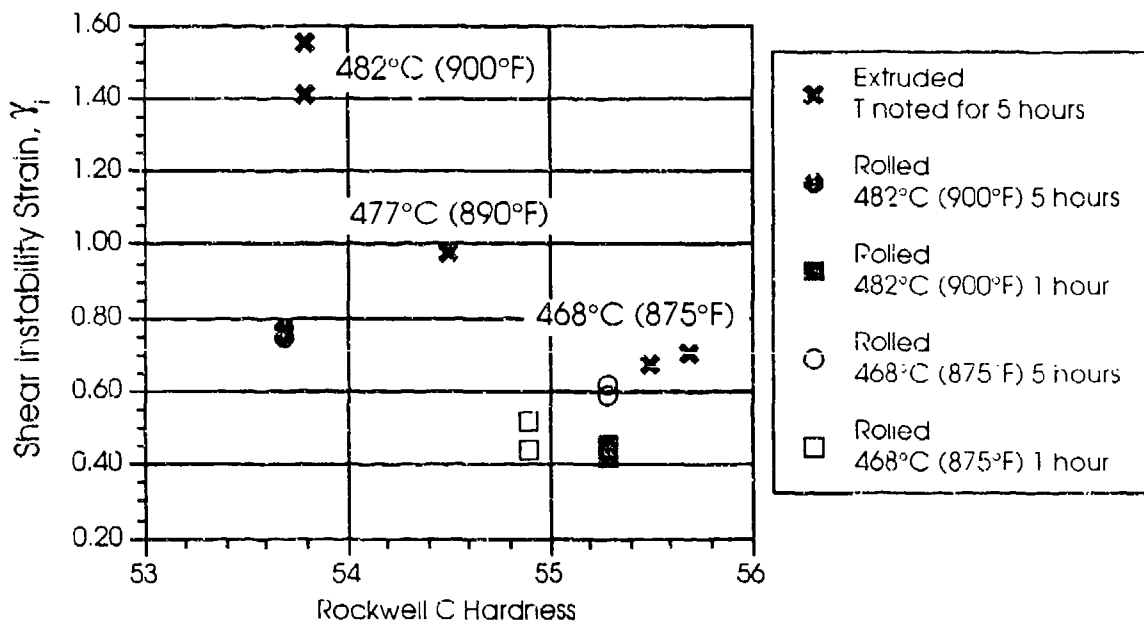


Figure 12: Shear Instability Strains for AerMet® 100 Steel for Various Ageing Treatments.

The improved shear resistance of this secondary hardening steel (compared to that of quenched and tempered steels of the same hardness) is the key factor in providing improved ballistic performance at equivalent hardness. This improvement is achieved by delaying the onset of adiabatic shear bands, that play an important role in initiating the plugging mechanism of armor failure. The interaction of the fine scale microstructure ( $M_3C$  and  $M_2C$  precipitates in this case) with shear localization phenomena is not yet fully understood. Cowie

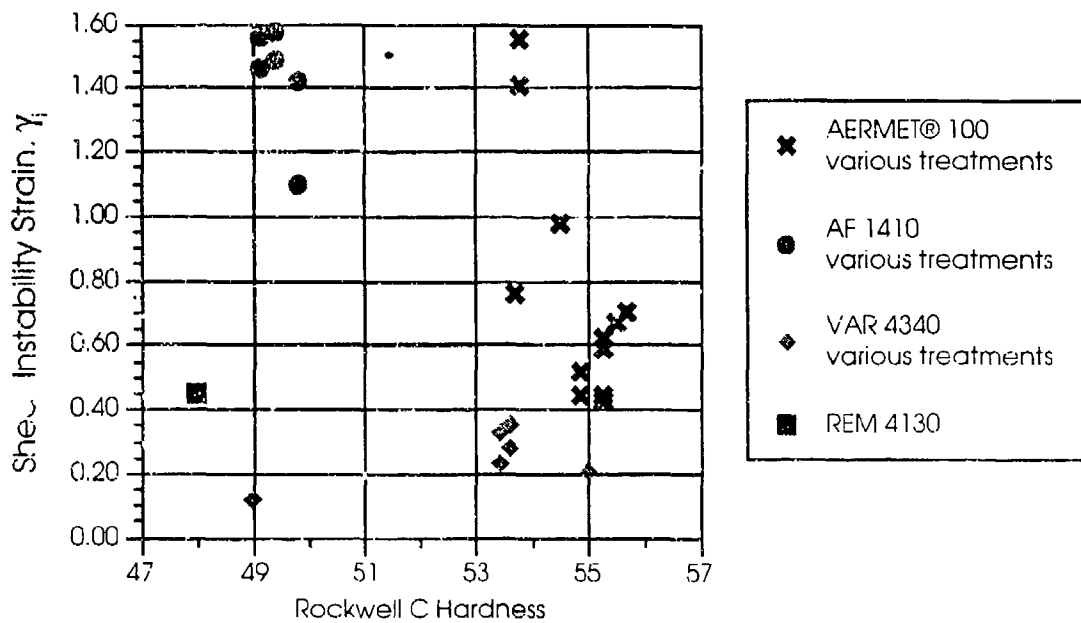


Figure 13: Comparison of Shear Instability Strains for Various High Strength Steels and AerMet® 100.

demonstrated that the ratio of carbide-size to carbide-separation-distance was the controlling factor at quasi-static strain rates in VAR 4340 steel.<sup>40</sup> However, at higher strain rates the same relationship does not hold, though the carbides still play an important role.<sup>42</sup> The unusually high instability strains measured for the extruded AerMet® 100 show promise for obtaining even better ballistic performance through processing and microstructural control.

The influence of microstructure is an important consideration in the design of armor steels. The mixed microstructure of M<sub>3</sub>C and M<sub>2</sub>C is more brittle than a microstructure comprised primarily of M<sub>2</sub>C carbides. From a microstructural standpoint, elimination of M<sub>3</sub>C carbides while precipitating M<sub>2</sub>C carbides in this class of armor steels is preferred. The former reduce fracture toughness and tend to promote brittle fracture, while the latter have the dual benefit of improving strength by impeding dislocation flow and increasing toughness through better interfacial cohesion with the matrix. These microstructural features are important to ballistic performance because they determine—in part—the plate's tendency to fail by brittle fracture and its resistance to localized adiabatic shear.

While processing AerMet® 100 to hardness levels greater than 55 HRC in combination with an overaged microstructure may not be feasible, it may be possible to design a new secondary hardening steel with an overaged microstructure and higher hardness. To this end, ARL-MD funded an effort with Northwestern University to design an armor steel possessing both the desired mechanical properties and a microstructure of overaged M<sub>2</sub>C carbides.<sup>43,44</sup> Ballistic tests of the new armor steel were initiated in the Fall of 1993 and should be completed by the end of 1994.

#### Stress Corrosion Cracking Tests

Atrens measured crack growth velocity in AerMet® 100 steel using a linear increasing stress test (LIST).<sup>45</sup> The findings of his study are graphed in Figure 14. At stress intensities below 20 MPa $\sqrt{m}$ , there was no apparent crack growth. Crack velocities for K<sub>I</sub> greater than 65 MPa $\sqrt{m}$  were not measured. Given the geometry of the cantilever beam specimen, it should be possible using Atrens' data to estimate time to failure.

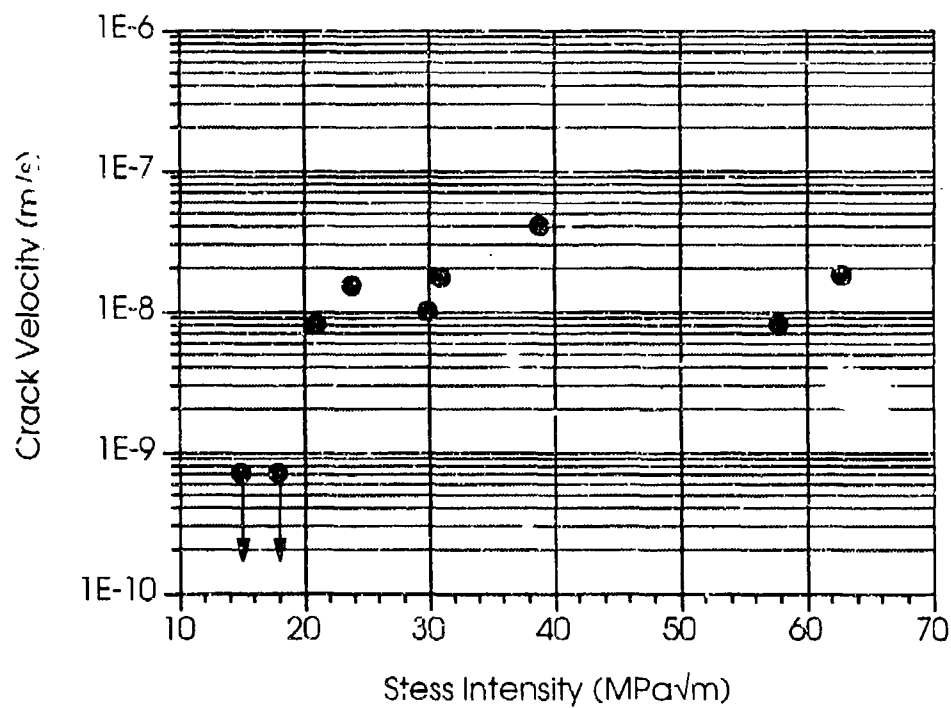


Figure 14: Atrens' Crack Velocity Data for AerMet® 100 Steel.

As a first approximation, consider crack growth rates to be constant. The only compelling reason for this assumption is to facilitate a first estimate of the time to failure. Crack growth usually proceeds as a two step process. First, proper conditions must be established at the crack tip. As the crack grows into the material, it will decelerate and arrest until sufficient hydrogen diffuses to the crack tip to reinitiate growth.

To aid comparison of Atrens' crack growth velocity data with cantilever beam data from this study and the NAWC study, two commercially available software packages—Mathematica by Wolfram Research and MathCad by MathSoft—were used to develop crack growth models. Although difficult to learn, Mathematica offered a greater variety of built in functions. MathCad offered fewer functions but has a better display interface including automatic dimensional analysis. Because MathCad offered sufficient functionality for the crack growth model with a more intuitive interface, it was selected to render the model.

The crack growth velocity is simply the incremental change in unit crack length during a unit of time:

$$v = \frac{da}{dt} \quad (3)$$

The time to failure is expressed as:

$$t_f = \int_0^{a_f} dt \quad (4)$$

Which can be rewritten:

$$t_f = \int_{a_i}^{a_f} \frac{1}{V} da \quad (5)$$

Atrens' data can be fit to a log linear equation like the following:<sup>16</sup>

$$v = \text{Constant} \cdot e^{mk} \quad (6)$$

Where:  $m = 3.667 \cdot 10^{-6} \frac{1}{\text{MPa}\sqrt{\text{m}}} = (4.03 \cdot 10^{-6} \frac{1}{\text{psi}\sqrt{\text{in}}})$

$$\text{Constant} = 1.235 \cdot 10^{-8} \frac{\text{m}}{\text{hr}} = (1.75 \cdot 10^{-3} \frac{\text{in}}{\text{hr}})$$

The Kies equation (2) used earlier to determine  $K$  as a function of flaw size,  $a$ , may now be substituted into equations 6 and 5 to produce an equation for failure time as a function of flaw size,  $a$ :

$$t_f = \int_{a_i}^{a_f} \frac{1}{\text{Constant} \cdot e^{\left(\frac{4.12 M}{B w^{3/2}} \sqrt{\frac{1}{a^3} - \frac{1}{a_f^3}}\right)}} da \quad (7)$$

The MathCad program implementing the solution to this equation is shown in Appendix B. Once the single calculation file was set up, it was relatively easy to introduce a matrix of initial stress intensity values to determine corresponding values for time to failure. Table 8 lists the predicted failure time based upon the cantilever beam specimen geometry, initial flaw size, and flaw size at fracture, along with the actual time to failure.

Table 8: Comparison of ARL•MD Cantilever Beam and Atrens' Linear Increasing Stress Test Data.

Initial Stress Intensity, $K_I$ MPa $\sqrt{m}$ (ksi/in)	Time to Failure (hours)	Predicted Failure Time (hours)	Predicted Time Actual Time
44 (40)	422.8	149.8	0.35
38 (35)	1200*	171.2	0.14
33 (30)	475.8	195.1	0.41
27 (25)	658.8	221.8	0.34
22 (20)	1155.2	252.1	0.22

These predictions are remarkably consistent with the actual time to failure given the fidelity usually associated with cantilever beam data and crack velocity measurements. The experimental time to failure for the specimen loaded to an initial stress intensity of 38 MPa $\sqrt{m}$  (35 ksi/in, marked with an \*) does not fit well with the other data because of crack bifurcation. The specimen loaded to 22 MPa $\sqrt{m}$  (20 ksi/in) does not fit the other data, presumably because 22 MPa $\sqrt{m}$  (20 ksi/in) is the apparent  $K_{ISCC}$  for AerMet® 100. Since the calculated times to failure are shorter than the actual times to failure, our assumption of constant crack growth needs to be considered in more detail. If crack growth decelerates because of a change in the environment at the crack tip, the time to failure would be greater.

## **7.0 Conclusions and Recommendations**

AerMet® 100 is very sensitive to ageing temperature. As a result, careful process control is required to ensure that the desired properties are obtained. Hardness tests are not a reliable measure of process control; the best indicators for process control are tensile and fracture toughness tests.

The ballistic performance of AerMet® 100 heat treated to achieve different microstructures provides valuable knowledge for use in future efforts to design high performance armor steels for specialized applications. Even if combinations of hardness greater than 55 HRC with toughness greater than 55 MPa $\sqrt{\text{m}}$  (50 ksi $\sqrt{\text{in}}$ ) can be achieved, special care must be taken to ensure that the microstructure is contributing as much hardness as possible without introducing undesirable effects such as brittle fracture.

Although the peak hardened condition of AerMet® 100 is not the optimum microstructure for toughness limited applications, it has mechanical properties at least as good as other ultrahigh strength steels and superior ballistic performance against one of the small arms projectiles. Future efforts should be directed at producing a slightly overaged microstructure with optimized hardness.

AerMet® 100 is susceptible to stress corrosion cracking. Although fracture toughness is an important consideration for design and materials selection, a more important limitation is resistance to stress corrosion cracking. Using the  $K_{IC}$ , rather than  $K_{ISCC}$ , in a design calculation could lead to premature failure. In cases where  $K_{ISCC}$  may be exceeded, development of an inspection schedule that takes crack growth velocity into account is of critical importance.

AerMet® 100 has greater fracture toughness than conventional high strength steels so components fabricated from it can tolerate larger flaw sizes. In addition, crack growth velocity of AerMet® 100 immersed in 3.5% sodium chloride is slower than for conventional high strength steels, permitting longer inspection intervals. Therefore, one for one substitution of AerMet® 100 for conventional high strength steels is recommended. However, substitution of AerMet® 100 in components scaled to achieve weight savings requires careful consideration.

## References

- 1 J.F. Mescall and H. Rogers, "The Role of Shear Instability in Ballistic Protection," *Innovations in Ultrahigh-Strength Steel Technology, Proceedings of the 34th Sagamore Army Materials Research Conference*, U.S. Army Materials Technology Laboratory, Watertown, MA, March 1990, pg. 287.
- 2 M. Azrin, J.G. Cowie, A.A. Anctil, and E.B. Kula, *Some Correlations Between Plate Shatter and Fracture Toughness*, U.S. Army Materials Technology Laboratory, MTL TR 87-9, February 1987.
- 3 T.S. Thomas and A.A. Anctil, *Characterization of Electroslag Remelted and Ladle Refined, Electric Furnace Melted 4340 Steel Armor*, J. Heat Treating, Vol 4, No. 4, December 1986, pp. 317-325.
- 4 P.G. Shewmon, *Transformations in Metals*. McGraw Hill, 1969, pg 351.
- 5 G.R. Speich, "Secondary Hardening Ultrahigh Strength Steels," *Innovations in Ultrahigh-Strength Steel Technology, Proceedings of the 34th Sagamore Army Materials Research Conference*, U.S. Army Materials Technology Laboratory, Watertown, MA, March 1990, pg. 94.
- 6 G.R. Speich, D.S. Dabkowski, and L.F. Porter, "Strength and Toughness of Fe-10Ni Alloys Containing C, Co, Mo, and Cr," *Metallurgical Transactions*, Volume 4, January 1973, pp. 303 - 315.
- 7 D.A. Porter and K.E. Easterling, *Phase Transformations in Metals and Alloys*, Van Nostrand Reinhold Co. Ltd, 1981, pg. 423.
- 8 D.A. Porter and K.E. Easterling, pg. 271
- 9 C. Shick, *Thermodynamics of Certain Refactory Compounds*, Academic Press, New York, 1966.
- 10 M. Grujicic, "Design of M<sub>2</sub>C Carbides for Secondary Hardening," *Innovations in Ultrahigh-Strength Steel Technology, Proceedings of the 34th Sagamore Army Materials Research Conference*, U.S. Army Materials Technology Laboratory, Watertown, MA, March 1990, pg. 223.
- 11 D.S. Dabkowski, P.J. Konkol, L.F. Porter, and A.M. Rathbone, *Nickel, Cobalt, Chromium Steel*, United States Patent 3,502,462 issued March 24, 1970.
- 12 C.D. Little and P.M. Machmeier, *High Strength Fracture Resistant Weldable Steels*, United States Patent 4,076,525 issued February 28, 1978.
- 13 R.M. Hemphill and D.E. Wert, *High Strength, High Fracture Toughness Structural Alloy*, United States Patent 5,087,415 issued February 11, 1992.

## References

- 14 Aerospace Material Specification 6532, Society of Automotive Engineers.
- 15 A. Magnée, J.M. Drapier, J. Dumont, D. Coutsouradis, and L. Habraken, *Cobalt Containing High Strength Steels*, Centre D'Information Du Cobalt, Brussels, 1974, pg. 35.
- 16 J. Kameda and C.J. McMahon Jr., Metallurgical Transactions. A, 1981, Vol. 12A, pg. 31.
- 17 J.F. Watton, *A Novel Hydrogen-Resistant UHS Steel*, Doctoral Thesis, Massachusetts Institute of Technology, 1987.
- 18 P. Buckley, M. Levy, J. Beatty, and R. Brown, "Hydrogen-Induced Stress Corrosion Cracking Susceptibility Analysis of Pitch Links from the AH-64 Apache Helicopter," *Proceedings of the Tri-Service Conference on Corrosion*. Plymouth, MA, May 1992, pp. 87 - 93.
- 19 M. Levy, P. Buckley, J. Beatty, R. Brown, R. Huie and K. Bhansali, "Failure Analysis of the Main rotor Retention Nut from the AH-64 Helicopter," *Proceedings of the Tri-Service Conference on Corrosion*. Plymouth, MA, May 1992, pp. 103 - 121.
- 20 V. Champagne, G. Wechsler, M.S. Pepi, and K. Bhansali, "Failure Analysis of the Apache Mixer Pivot Support," *Proceedings of the Tri-Service Conference on Corrosion*. Plymouth, MA, May 1992, pp. 123 - 138.
- 21 B.F. Brown and C.D. Beachem, "A Study of the Stress Factor in Corrosion Cracking by Use of the Precracked Cantilever-Beam Specimen," *Corrosion Science*, 5, 1965, pp. 745-750.
- 22 J.S. Montgomery and G.B. Olson, "M2C Carbide Precipitation in AF1410," *1992 Speich Symposium Proceedings*, Montreal, Canada, 1992, pp. 177 - 214.
- 23 J.H. Graves, and J.H. Beatty, "Ballistic Performance and Adiabatic Shear Behavior of AerMet™ 100 Steel," *40th U.S. Army Sagamore Materials Research Conference Proceedings*, Editors: M.G.H. Wells and J.H. Beatty, September 1994. (In-Press).
- 24 Contract number DAAL04-92-M-0164 dated 13 January 1992, Carpenter Technology Corporation, Order Number W93077.
- 25 *Test Methods for Rockwell Hardness and Rockwell Superficial Hardness of Metallic Materials*. Annual Book of ASTM Standards. American Society for Testing and Materials, Philadelphia, PA. 1993, Volume 03.01, pp. 184 - 197.

## References

- 26 P.M. Novotny, "An Aging Study of Carpenter AerMet® 100 Alloy," 1992 *Speich Symposium Proceedings*, Montreal, Canada, 1992, pp. x.
- 27 M. Schmidt and M. Gore, "Solution Treatment Effects in AF 1410 Steel," *Innovations in Ultrahigh-Strength Steel Technology, Proceedings of the 34th Sagamore Army Materials Research Conference*, U.S. Army Materials Technology Laboratory, Watertown, MA, March 1990, pp 407 - 424.
- 28 *Test Method for Vickers Hardness of Metallic Materials*. Annual Book of ASTM Standards. American Society for Testing and Materials, Philadelphia, PA. 1993. Volume 03.01. pp. 277 - 285.
- 29 *Standard Test Methods for Tension Testing of Metallic Materials*. Annual Book of ASTM Standards. American Society for Testing and Materials, Philadelphia, PA. 1993. Volume 03.01. pp. 130 - 149.
- 30 *Test Method for Plane-Strain Fracture Toughness of Metallic Materials*. Annual Book of ASTM Standards. American Society for Testing and Materials, Philadelphia, PA. 1993. Volume 03.01. pp. 509 - 539.
- 31 *Standard Test Methods for Notched Bar Impact Testing of Metallic Materials*. Annual Book of ASTM Standards. American Society for Testing and Materials, Philadelphia, PA. 1993. Volume 03.01. pp. 206 - 226.
- 32 J. Kozol and C.E. Neu, *Stress Corrosion Susceptibility of Ultra-High Strength Steels for Naval Aircraft Applications*. Naval Air Warfare Center, Warminster, PA, Report No. NAWCADWAR-92018-60, January 1992.
- 33 C.D. Beachem and B.F. Brown, "A Comparison of Three Precracked Specimens for Evaluating the Susceptibility of High-Strength Steel to Stress Corrosion Cracking," *Stress Corrosion Testing*, ASTM STP 425, December 1967, pp. 31-40.
- 34 G.E. Dieter, *Mechanical Metallurgy*, McGraw Hill, 1976. pp. 272-275.
- 35 M.A. Meyers and K.K. Chawla, *Mechanical Metallurgy*, Prentice-Hall, 1984, pp. 649-652.
- 36 W.F. Brown and J.E. Srawley, *Plane Strain Crack Toughness Testing of High Strength Metallic Materials*, American Society for Testing and Materials Special Technical Publication (STP) 410, December 1967.

## References

- 37 J.A. Kies, H.L. Smith, H.E. Romine, and H. Berstein, "Fracture Testing of Weldments," ASTM STP 381: *Fracture Toughness Testing and Its Applications*. American Society For Testing and Materials, Philadelphia, PA, 1965, pg. 328.
- 38 MIL-STD-662E, *V50 Ballistic Test for Armor*. U.S. Army Research Laboratory, Materials Directorate, Watertown, MA, 22 January 1987.
- 39 J. Kozoi and C.E. Neu, *Stress Corrosion Susceptibility of Ultra-High Strength Steels for Naval Aircraft Applications*. Naval Air Warfare Center, Warminster, PA, Report No. NAWCADWAR-92018-60, January 1992.
- 40 J.G. Cowie, M. Azrin, M. and G.B. Olson, "Microvoid Formation during Shear Deformation of Ultrahigh Strength Steels," *Metall. Trans. A.*, **20A**, January, 1989, pp. 143-153.
- 41 J.H. Beatty and M. Azrin, "Correlation of Ballistic Performance to Shear Instability Studies in High Strength Steel," *1992 U.S. Army Science Conference Proceedings*. eds. Kamely, Bannister, Sasmor, pp. 393-404.
- 42 J.H. Beatty, L.W. Meyer, M.A. Meyers, and S. Nemat-Nasser, "Formation of Controlled Adiabatic Shear Bands in AISI 4340 High Strength Steels," *Shock Waves and High Strain Rate Phenomena in Materials*, editor: M. Meyers, Murr, Staudhammer, Markel Dekker pub., 1991 from Explomet 90, UCSD, LaJolla, CA, AUG12-17 1990.
- 43 G.B. Olson, and T.A. Stephenson, *Design of Advanced Steels for Armor Applications*, Final Report for Contract DAAL04-91-C-0073, July 1993.
- 44 G.B. Olson, "Beyond AerMet® 100: Systems Design of High Performance Steels," *40th U.S. Army Sagamore Materials Research Conference Proceedings*. Editors: M.G.H. Wells and J.H. Beatty, September 1994.
- 45 A. Atrens, Facsimile Transmission from the University of Queensland, Brisbane, Australia, July, 1992. (Private communication)
- 46 D.P. Willam , International Journal of Fracture, 1973, Vol 9, No. 1, pg. 63.

## Appendix A

ARL-MD Ballistic Test Number 151-92.  
.0156 inch thick AerMet 100™ Steel versus U.S. 0.50 caliber AP M2 projectile.  
(Austenitized @ 1625°F, 1 hour, oil quench; -100°F, 1 hour, air warm; Aged @ 875°F, 5 hours, air cool.)



Front Side



Back Side

## Appendix A

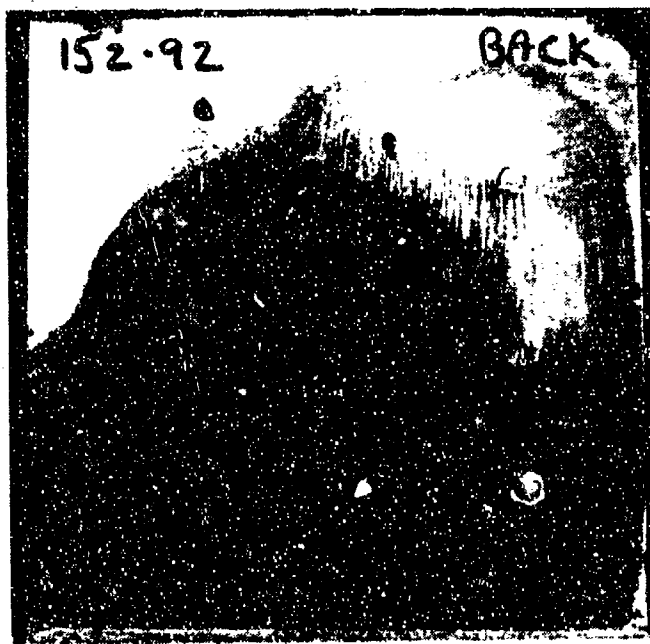
ARL•MD Ballistic Test Number 152-92.

0.230 inch thick AerMet 100™ Steel versus U.S. 0.50 caliber AP M2 projectile.

(Austenitized @ 1625°F, 1 hour, oil quench; -100°F, 1 hour, air warm; Aged @ 900°F, 5 hours, air cool.)



Front Side



Back Side

## Appendix A

ARL•MD Ballistic Test Number 153-92.

0.350 inch thick AerMet 100™ Steel versus U.S. 0.50 caliber AP M2 projectile.  
(Austenitized @ 1625°F, 1 hour, oil quench; -100°F, 1 hour, air warm; Aged @ 875°F, 5 hours, air cool.)



Front Side



Back Side

## Appendix A

ARL•MD Ballistic Test Number 154-92.  
0.375 inch thick AerMet 100™ Steel versus U.S. 0.50 caliber AP M2 projectile.  
(Austenitized @ 1625°F, 1 hour, oil quench; -100°F, 1 hour, air warm; Aged @ 900°F, 5 hours, air cool.)



Front Side



Back Side

## Appendix A

ARL•MD Ballistic Test Number 155-92.

0.483 inch thick AerMet 100™ Steel versus U.S. 0.50 caliber AP M2 projectile.  
(Austenitized @ 1625°F, 1 hour, oil quench; -100°F, 1 hour, air warm; Aged @ 875°F, 5 hours, air cool.)



Front Side



Back Side

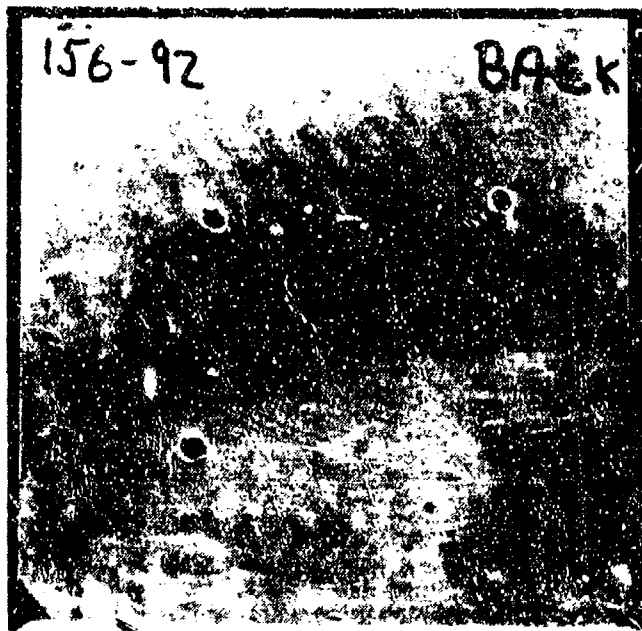
## Appendix A

ARL•MD Ballistic Test Number 156-92.

0.488 inch thick AerMet 100™ Steel versus U.S. 0.50 caliber AP M2 projectile.  
(Austenitized @ 1625°F, 1 hour, oil quench; -100°F, 1 hour, air warm; Aged @ 900°F, 5 hours, air cool.)



Front Side



Back Side

## Appendix A

ARL•MD Ballistic Test Number 001-93.  
0.453 inch thick AerMet 100™ Steel versus U.S. 0.50 caliber AP M2 projectile.  
(Austenitized @ 1625°F, 1 hour, air cool; -100°F, 1 hour, air warm; Aged @ 900°F, 5 hours, air cool.)



Front Side



Back Side

## Appendix A

AK-47 Ballistic Test Number 002-93.

0.481 inch thick AerMet<sup>®</sup> Steel versus U.S. 0.50 caliber AP M2 projectile.

(Austenitized @ 1625°F, 1 hour; air cool to 100°F, 1 hour, air warm; Aged @ 875°F, 5 hours, air cool.)



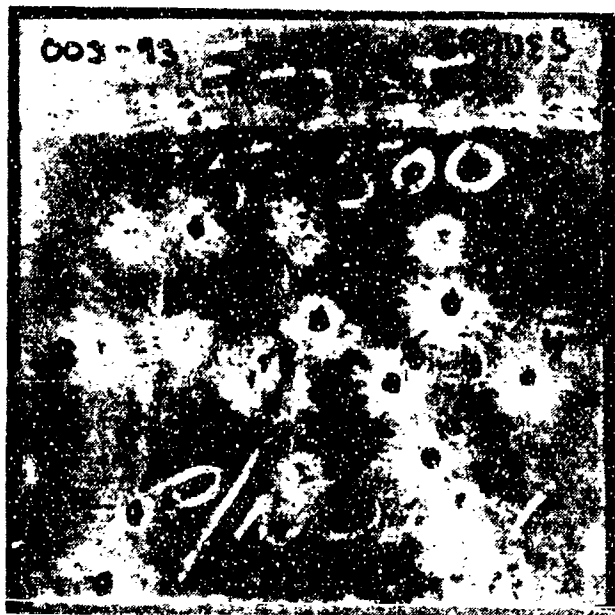
Front Side



Back Side

## Appendix A

ARL•MD Ballistic Test Number 003-93.  
0.470 inch thick AerMet 100™ Steel versus U.S. 0.50 caliber AP M2 projectile.  
(Austenitized @ 1625°F, 1 hour, air cool; -100°F, 1 hour, air warm; Aged @ 900°F, 1 hour, air cool.)



Front Side



Back Side

## Appendix A

ARL•MD Ballistic Test Number 004-93.

0.467 inch thick AerMet 100™ Steel versus U.S. 0.50 caliber AP M2 projectile.  
(Austenitized @ 1625°F, 1 hour, air cool; -100°F, 1 hour, air warm; Aged @ 875°F, 1 hour, air cool.)



Front Side



Back Side

## Appendix A

ARL-MD Ballistic Test Number 005-93.

0.330 inch thick AerMet 100™ Steel versus U.S. 0.50 caliber AP M2 projectile.  
(Austenitized @ 1625°F, 1 hour, air cool. 100°F 1 hour, air warm; Aged @ 900°F, 5 hours, air cool.)



Front Side



Back Side

## Appendix A

ARL•MD Ballistic Test Number 006-93.  
0.364 inch thick AerMet 100™ Steel versus U.S. 0.50 caliber AP M2 projectile.  
(Austenitized @ 1625°F, 1 hour, air cool; -100°F, 1 hour, air warm; Aged @ 875°F, 5 hours, air cool )



Front Side



Back Side

## Appendix A

ARL-MD Ballistic Test Number 007-93.

0.309 inch thick AerMet 100™ Steel versus U.S. 0.50 caliber AP M2 projectile.  
(Austenitized @ 1625°F, 1 hour, air cool; -100°F, 1 hour, air warm; Aged @ 900°F, 1 hour, air cool.)



Front Side



Back Side

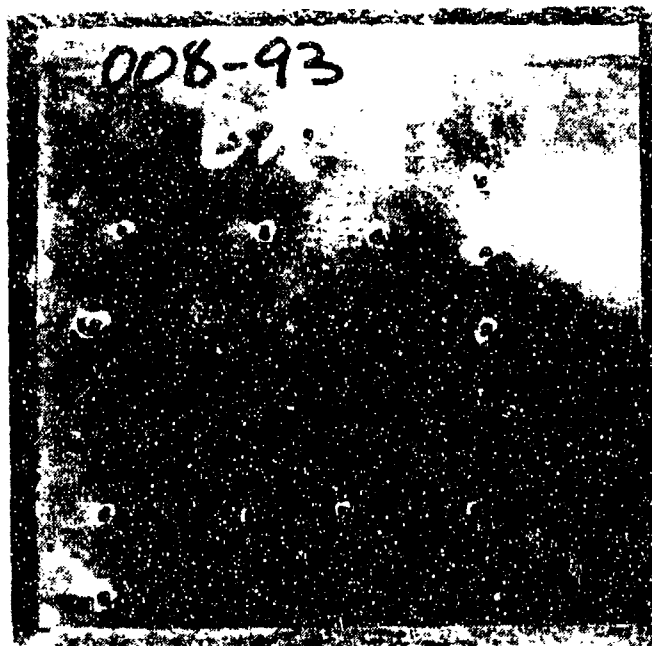
## Appendix A

ARL-MD Ballistic Test Number 008-93.

0.156 inch thick AerMet 100™ Steel versus U.S. 0.30 caliber AP M2 projectile.  
(Austenitized @ 1625°F, 1 hour, air cool. 100°F, 1 hour, air warm; Aged @ 900°F, 5 hours, air cool.)



Front Side



Back Side

## Appendix A

ARL-MD Ballistic Test Number 009-93.  
0.355 inch thick AerMet 100™ Steel versus U.S. 0.50 caliber AP M2 projectile.  
(Austenitized @ 1625°F, 1 hour, air cool; -100°F, 1 hour, air warm; Aged @ 875°F, 1 hour, air cool.)



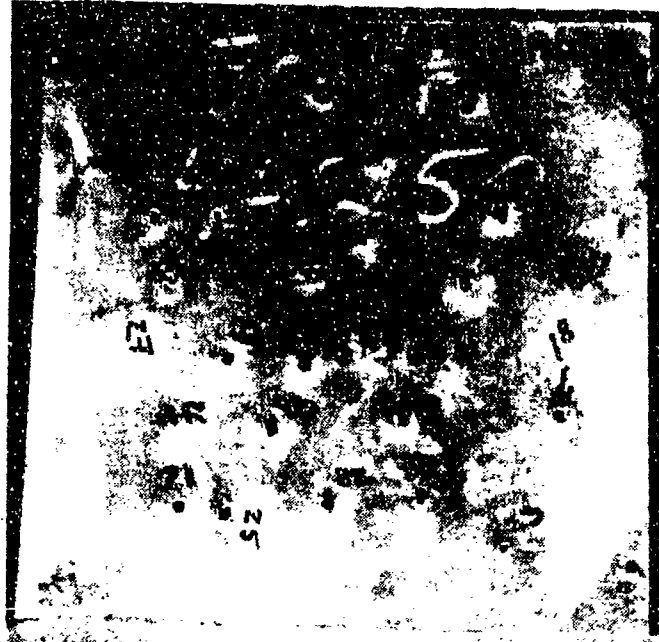
Front Side



Back Side

## Appendix A

ARL•MD Ballistic Test Number 010-93.  
0.135 inch thick AerMet 100™ Steel versus U.S. 0.30 caliber AP M2 projectile.  
(Austenitized @ 1625°F, 1 hour, air cool; 100°F 1 hour, air warm; Aged @ 875°F, 5 hours, air cool.)



Front Side



Back Side

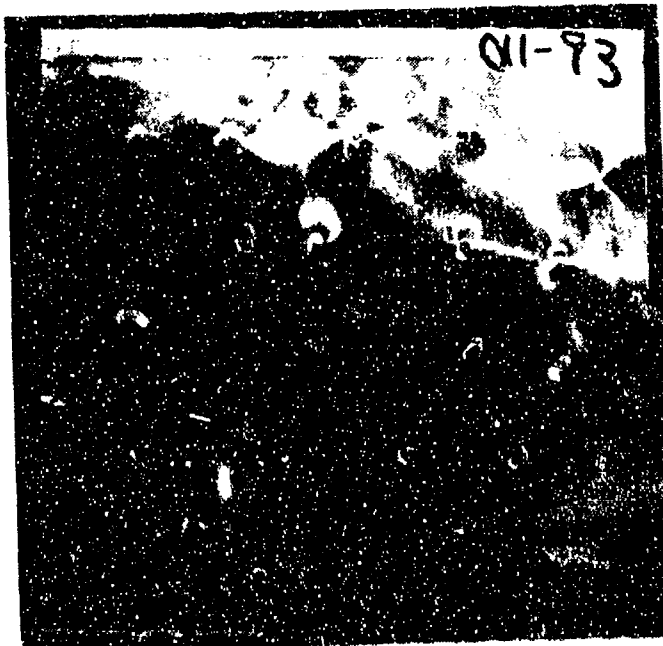
## Appendix A

ARL•MD Ballistic Test Number 011-93.

0.146 inch thick AerMet 100™ Steel versus U.S. 0.30 caliber AP M2 projectile.  
(Austenitized @ 1625°F, 1 hour, air cool; -100°F, 1 hour, air warm; Aged @ 900°F, 1 hour, air cool.)



Front Side



Back Side

## Appendix A

ARL-MD Ballistic Test Number 012-93.

0.197 inch thick AerMet 100™ Steel versus U.S. 0.30 caliber AP M2 projectile.

(Austenitized @ 1625°F, 1 hour, air cool; -100°F 1 hour, air warm; Aged @ 875°F, 1 hour, air cool.)



Front Side



Back Side

## Appendix A

ARL-MD Ballistic Test Number 013-93.  
0.191 inch thick AerMet 100™ Steel versus U.S. 0.30 caliber AP M2 projectile.  
(Austenitized @ 1625°F, 1 hour, air cool, -100°F 1 hour air warm; Aged @ 875°F, 5 hours, air cool.)



Front Side



Back Side

## Appendix A

ANL • MI • Ballistic Test Number 014-93.

0.155 inch thick AerMet 100™ Steel versus U.S. 0.30 caliber AP M2 projectile.  
(Austenitized @ 1625°F, 1 hour; 1100°F, 1 hour, air warm; Aged @ 900°F, 5 hours, air cool.)



Front Side



Back Side

## Appendix B

$$\text{MPa} \equiv 10^6 \text{ Pa} \quad \text{ksi} \equiv 1000 \text{ psi}$$

furlong  $\equiv 220 \text{ yd}$

fortnight  $\equiv 14 \text{ day}$

$$c(a, W) := 1 - \frac{a}{W}$$

$$K(a, M, B, W) := \frac{4.12 \cdot M \cdot \sqrt{\frac{1}{c(a, W)^3}}}{B \cdot W^2}$$

Factor  $\equiv 1$

$$\text{slope} := 4.03045 \cdot 10^{-6} \cdot (\text{psi} \cdot \sqrt{\text{in}})^{-1}$$

$$\text{Const} := 1.752324 \cdot 10^{-3} \frac{\text{in}}{\text{hr}}$$

$$\text{Velocity}(K) := \text{Factor} \cdot \text{Const} \cdot e^{\text{slope} \cdot K}$$

$$a_i := 0.125 \cdot \text{in} \quad W := 1.00 \cdot \text{in} \quad B = \frac{W}{2} \quad K_C := 115 \cdot \text{ksi} \cdot \sqrt{\text{in}}$$

$$a_i = 0.318 \cdot \text{cm} \quad W = 2.54 \cdot \text{cm} \quad B = 1.27 \cdot \text{cm} \quad K_C = 126.364 \cdot \text{MPa} \cdot \sqrt{\text{m}}$$

$$M := 0 \cdot \text{in} \cdot \text{lbf} \quad K_i := 40 \cdot \text{ksi} \cdot \sqrt{\text{in}}$$

$$a_f := a_i \quad K_i = 43.953 \cdot \text{MPa} \cdot \sqrt{\text{m}}$$

$$M_i := \text{root}(K(a_i, M, B, W) - K_i, M)$$

$$M_i = 5352 \cdot \text{in} \cdot \text{lbf}$$

$$M_i = 6166 \cdot \text{cm} \cdot \text{kgf}$$

$$a_f := \text{root}(K(a_f, M_i, B, W) - K_C, a_f)$$

$$a_f = 0.475862 \cdot \text{in}$$

$$a_f = 1.20869 \cdot \text{cm}$$

$$a_f = 0.00006 \cdot \text{furlong}$$

$$t_f := \int_{a_i}^{a_f} \frac{1}{\text{Velocity}(K(a, M_i, B, W))} da$$

$$t_f = 0.446 \cdot \text{fortnight}$$

$$t_f = 149.727 \cdot \text{hr}$$

DISTRIBUTION LIST

No. of Copies	To
1	Office of the Under Secretary of Defense for Research and Engineering, The Pentagon, Washington, DC 20301
1	Director, U.S. Army Research Laboratory, 2800 Powder Mill Road, Adelphi, MD 20783-1197
1	ATTN: AMSRL-OP-SD-TP, Technical Publishing Branch
1	AMSRSL-OP-SD-TA, Records Management
1	AMSRSL-OP-SD-TL, Technical Library
2	Commander, Defense Technical Information Center, Cameron Station, Building 5, 5010 Duke Street, Alexandria, VA 23304-6145 ATTN: DTIC-FDAC
1	MIA/CINDAS, Purdue University, 2595 Yeager Road, West Lafayette, IN 47905
1	Commander, Army Research Office, P.O. Box 12211, Research Triangle Park, NC 27709-2211 ATTN: Information Processing Office
1	Commander, U.S. Army Materiel Command, 5001 Eisenhower Avenue, Alexandria, VA 22333 ATTN: AMCSCI
1	Commander, U.S. Army Materiel Systems Analysis Activity, Aberdeen Proving Ground, MD 21005 ATTN: AMXS1-MP, H. Cohen
1	Commander, U.S. Army Missile Command, Redstone Arsenal, AL 35809 ATTN: AMSMI-RD-CS-R/Doc
2	Commander, U.S. Army Armament, Munitions and Chemical Command, Dover, NJ 07801 ATTN: Technical Library
1	Commander, U.S. Army Natick Research, Development and Engineering Center, Natick, MA 01760-5010 ATTN: SATNC-MI, Technical Library
1	Commander, U.S. Army Satellite Communications Agency, Fort Monmouth, NJ 07703 ATTN: Technical Document Center
1	Commander, U.S. Army Tank-Automotive Command, Warren, MI 48397-5000 ATTN: AMSTA-ZSK 1 AMSTA-TSL, Technical Library
1	President, Airborne, Electronics and Special Warfare Board, Fort Bragg, NC 28307 ATTN: Library
1	Director, U.S. Army Research Laboratory, Weapons Technology, Aberdeen Proving Ground, MD 21005-5066 ATTN: AMSRL-WT

No. of Copies	To
	Commander, Dugway Proving Ground, UT 84022
1	ATTN: Technical Library, Technical Information Division
	Commander, U.S. Army Research Laboratory, 2800 Powder Mill Road, Adelphi, MD 20783
1	ATTN: AMSRL-SS
	Director, Benet Weapons Laboratory, LCWSL, USA AMCCOM, Watervliet, NY 12189
1	ATTN: AMSMC-LCB TL
1	AMSMC-LCB-R
1	AMSMC-LCB-RM
1	AMSMC-LCB-RP
	Commander, U.S. Army Foreign Science and Technology Center, 220 7th Street, N.E., Charlottesville, VA 22901-5396
3	ATTN: AFRTC, Applied Technologies Branch, Gerald Schlesinger
	Commander, U.S. Army Aeromedical Research Unit, P.O. Box 577, Fort Rucker, AL 36360
1	ATTN: Technical Library
	U.S. Army Aviation Training Library, Fort Rucker, AL 36360
1	ATTN: Building 5906-5907
	Commander, U.S. Army Agency for Aviation Safety, Fort Rucker, AL 36362
1	ATTN: Technical Library
	Commander, Clarke Engineer School Library, 3202 Nebraska Ave., N, Fort Leonard Wood, MO 65473-5000
1	ATTN: Library
	Commander, U.S. Army Engineer Waterways Experiment Station, P.O. Box 631, Vicksburg, MS 39180
1	ATTN: Research Center Library
	Commandant, U.S. Army Quartermaster School, Fort Lee, VA 23801
1	ATTN: Quartermaster School Library
	Naval Research Laboratory, Washington, DC 20375
1	ATTN: Code 6384
	Chief of Naval Research, Arlington, VA 22217
1	ATTN: Code 471
	Commander, U.S. Air Force Wright Research & Development Center, Wright-Patterson Air Force Base, OH 45433-6523
1	ATTN: WRDC/MLLP, M. Forney, Jr.
1	WRDC/MLBC, Mr. Stanley Schulman
	U.S. Department of Commerce, National Institute of Standards and Technology, Gaithersburg, MD 20899
1	ATTN: Stephen M. Hsu, Chief, Ceramics Division, Institute for Materials Science and Engineering

No. of Copies	To
1	Committee on Marine Structures, Marine Board, National Research Council, 2101 Constitution Avenue, N.W., Washington, DC 20418
1	Materials Sciences Corporation, Suite 250, 500 Office Center Drive, Fort Washington, PA 19034
1	Charles Stark Draper Laboratory, 555 Technology Square, Cambridge, MA 02139
	Wyman-Gordon Company, Worcester, MA 01601
1	ATTN: Technical Library
	General Dynamics, Convair Aerospace Division, P.O. Box 748, Fort Worth, TX 76101
1	ATTN: Mfg. Engineering Technical Library
	Plastics Technical Evaluation Center, PLASTEC, ARDEC, Bldg. 355N, Picatinny Arsenal, NJ 07806-5000
1	ATTN: Harry Pebly
1	Department of the Army, Aerostructures Directorate, MS-266, U.S. Army Aviation R&T Activity - AVSCOM, Langley Research Center, Hampton, VA 23665-5225
1	NASA - Langley Research Center, Hampton, VA 23665-5225
	U.S. Army Vehicle Propulsion Directorate, NASA Lewis Research Center, 2100 Brookpark Road, Cleveland, OH 44135-3191
1	ATTN: AMSRL-VP
	Director, Defense Intelligence Agency, Washington, DC 20340-6053
1	ATTN: ODT-5A (Mr. Frank Jaeger)
	U.S. Army Communications and Electronics Command, Fort Monmouth, NJ 07703
1	ATTN: Technical Library
	U.S. Army Research Laboratory, Electronic Power Sources Directorate, Fort Monmouth, NJ 07703
1	ATTN: Technical Library
	Commander, U.S. Army Aviation and Troop Command, Aviation Research and Technology Activity, Aviation Applied Technology Directorate, Fort Eustis, VA 23604-5577
1	ATTN: AMSAT-R-TV, Mr. G. McAllister
1	AMSAT-R-TV, Mr. L. T. Burrows
1	AMSAT-R-TV, Mr. H. Holland
	Director, Combat Developments, U.S. Army Aviation Center, Fort Rucker, AL 36362-5000
1	ATTN: ATZQ-CD, Mr. R. S. McCabe

No. of  
Copies

To

---

Commander, U.S. Army Aviation and Troop Command, 4300 Goodfellow Boulevard, St. Louis,  
MO 63120-1798

- 1 ATTN: SFAE-AV-ASH, COL J. T. Huey
- 1 SFAE-AV, MG D. Irby, Jr.
- 1 SFAE-AV-SOA, LTC M. W. Rogers
- 1 SFAE-AV-AAH, COL S. L. Deloach
- 1 SFAE-AV-BH, LT COL J. Lanier
- 1 SFAE-AV-AEC, COL T. E. Reinkober
- 1 SFAE-AV-RAH, BG O. L. Mullen
- 1 SFAE-AV-CH, COL R. Williams
- 1 SFAE-AV-RAH-TV, M. Smith
- 1 AMSAT-R-ESC, Mr. G. Kovacs

Commander, U.S. Air Force Wright Research and Development Center, Wright-Patterson Air  
Force Base, OH 45433-6553

- 1 ATTN: WL/FIES, Mr. A. Kurtz
- 1 WL/FIVS/SURVIAC, Mr. J. Vice

Commander, Naval Surface Warfare Center, Dahlgren Laboratory, Dahlgren, VA 22448

- 1 ATTN: Code G-22, Dr. B. Smith

Commander, Naval Weapons Center, China Lake, CA 93555-6001

- 1 ATTN: Code 31801, Mr. J. R. Bates
- 1 C2183, Mr. J. Duzan
- 1 C2183, Mr. L. Budd

Commander, Naval Postgraduate School, Monterey, CA 93943

- 1 ATTN: Code 67BP, Prof. R. E. Ball

U.S. Secret Service Technical Development and Planning Division, 1301 L. Street, N.W.,  
Room 800, Washington, DC 20005

- 1 ATTN: Timothy Thomas

LRA Laboratories, Inc., 18195A East McDurmott Street, Irvine, CA 92714

- 1 ATTN: Dr. L. Raymond

Jet Propulsion Laboratory, California Institute of Technology, 4800 Oak Grove Drive,  
Pasadena, CA 91109

- 1 ATTN: Dr. M. Adams

- 1 Center for Naval Analysis, 4401 Fort Avenue, P.O. Box 16268, Alexandria, VA 22302-0268

Naval Air Engineering Center, Lakehurst, NJ 08733

- 1 ATTN: K. Megerle, SESD Code 5314 KM
- 1 G. Fisher, SESD Code MT-14

National Center of Excellence in Metal-Working Technology, Metal-Working Technology, Inc.,  
1450 Scalp Avenue, Johnstown, PA 15904

- 1 ATTN: L. Otto

---

No. of  
Copies

To

---

Wright Laboratories, Wright-Patterson Air Force Base, OH 45433-6533

1 ATTN: WL/MLSE, C. Harmsworth  
WL/MLSE, J. Coate  
WL/MLL.M, J. Petrak

Vought Corporation, P. O. Box 226144, Dallas, TX 75222

1 ATTN: Chief of Materials and Processes  
1 D. Peterson, Advanced Tech. Center

Grumman Aerospace Corporation, Bethpage, NY 11714

1 ATTN: Chief of Materials and Processes  
1 P. Adler, Mail Stop A02-26  
1 S. Demay, PL12, Dept. 441  
1 J. Kennedy, Mail Stop A02-26  
1 P. Shaw, Mail Stop A04-12  
1 J. Greenspan, Mail Stop, A04-12

Lockheed Aeronautical Systems Company, 86 South Cobb Drive, Zone 150, Marietta,  
GA 30063-0199

1 ATTN: D. Richardson, Dept. 73-C2 (Zone 0199)  
1 D. Chellman  
1 Chief of Materials and Processes  
1 J. Whitehead

Naval Air Systems Command, Jefferson Plaza One, Washington, DC 20361-5300

1 ATTN: S. Bettadupur, AIR-5304D  
1 M. Dubberly, AIR-5302  
1 J. Collins, AIR-5304  
1 H. Varmali, AIR-5304  
1 J. Thompson, AIR-5304C  
1 W. Koegel, AIR-5304D  
1 L. Sloter, AIR-536T

Naval Air Warfare Center Aircraft Division, Warminster, PA 18974-5000

1 ATTN: J. Kozel, Code 6063  
1 Technical Library, Code 8131

Martin Marietta Laboratories, Martin Marietta Corporation, 1450 S. Rolling Road,  
Baltimore, MD 21227-3898

1 ATTN: J. Green

Boeing Defense/Space Group, Helicopter Division, P.O. Box 16856, Philadelphia,  
PA 19142

1 ATTN: P. McIntyre, Mail Stop P38-21  
1 B. Thompson, Mail Stop P38-50

Office of Naval Research, Materials Engineering Division, 800 N. Quincy Street, Arlington,  
VA 22217-5000

1 ATTN: G. Yoder, Code 1311

No. of  
Copies

To

1 Professor Gregory B. Olson, Materials Science and Engineering, 2030 Tech. Institute,  
Northwestern University, Evanston, IL 60208-3108

Carpenter Technology Corporation, Carpenter Steel Division, Reading, PA 19603-0662  
1 ATTN: R. M. Hemphill, Supervisor Tool & Alloy R&D

McDonnell Aircraft Company, McDonnell Douglas Corp., P.O. Box 5116, St. Louis, MO 63166  
1 ATTN: Chief of Materials and Processes  
1 K. K. Sankaran, Mail Code 1021310  
1 R. Newcomer, Mail Code 1021310

Douglas Aircraft Company, McDonnell Douglas Corp., 3855 Lakewood Blvd., Long Beach,  
CA 90846  
1 ATTN: Chief of Materials and Processes

Northrop Corporation, Aircraft Division, 1 Northrop Avenue, Hawthorne, CA 90250-3277  
1 ATTN: M. Rommel, 3872-62  
1 Chief of Materials and Processes

Rockwell International Corporation, North American Aircraft Division, P.O. Box 92098,  
Los Angeles, CA 90009  
1 ATTN: Chief of Materials and Processes

Boeing Aerospace Co., Boeing Military Airplane Development, P.O. Box 3999, Seattle,  
WA 98124  
1 ATTN: Chief of Materials and Processes

Boeing Aircraft Company, 3801 South Oliver Street, Wichita, KS 67210  
1 ATTN: Chief of Materials and Processes

General Dynamics, Ft. Worth Division, P.O. Box 748, Fort Worth, TX 67101  
1 ATTN: Chief of Materials and Processes  
1 Susan Kiehl, MZ 2853

Sikorsky Aircraft, 6900 Main Street, Stratford, CT 06601-1381  
1 ATTN: Chief of Materials and Processes  
1 T. Murphy, Mail Stop S312A

Boeing Commercial Airplane Group, P.O. Box 3707, Seattle, WA 98124  
1 ATTN: D. Walleem, Mail Stop 73-44

Textron Lycoming, 550 S. Main Street, Stratford, CT 06497-2452  
1 ATTN: V. Nangia, Manager, Advanced Materials Tech. Lab.

1 Dianne Chong, McDonnell Douglas Missile Systems, M/C 1063246, P.O. Box 516,  
St. Louis, MO 63166-0516

Director, U.S. Army Research Laboratory, Watertown, MA 02172-0001  
2 ATTN: AMSRL-OP-WT-IS, Technical Library  
5 Author